FACULDADE DE ENGENHARIA DA UNIVERSIDADE DO PORTO

# Material Parameter Extraction from Reflection Measurements

**Rui Feio**

Mestrado Integrado em Engenharia Eletrotécnica e de Computadores

Supervisor: Prof. Sérgio Reis Cunha - FEUP

Co-Supervisor: Luís Rolo - ESTEC-ESA

Co-Supervisor: Elena Saenz - ESTEC-ESA

January 27, 2017

© Rui Feio, 2017

# Abstract

The presented work aims to accurately extract the complex permittivity of non-magnetic materials by means of reflection measurements only.

The method employed solves the problem unambiguously by means of a root-finding iterative algorithm that requires no previous knowledge of the dielectric constant nor more than a single sample of the material. However, precise knowledge of the thickness of the sample used is needed.

Measurements of S11 parameters are performed over a frequency band in free-space and compared to an analytical model, in order to arrive at a final solution.

Different facilities are used for measurement, as well as different materials, in order to validate results.

Finally, an uncertainty budget is developed in order to characterize the precision associated with the results.

The method proved to extract values for permittivity extremely close to the ones referenced in literature and with an uncertainty in the order of magnitude of $10^{-2}$.

# Acknowledgments

In English,

I would like to start by expressing my gratitude to Dennis Breeveld from KLOK and Steven Sablerolle from Metrology, for taking time out of their work to help me with my work.

Secondly, I am deeply grateful to the work environment provided for me in order to develop my work. All of the people from Antenna Section at ESTEC not only proved helpful whenever I needed them, but also made the workplace somewhere I actually looked forward to being there everyday. Regarding this matter I must give out a very special thanks to Luís Rolo and Elena Saenz for their precious help along each step of the way, Przemyslaw Radzik for his companionship and advice, Eric van der Houwen for his good mood and helpful attitude, and Peter de Maagt for creating a friendly work environment that I only hope my future jobs will live up to. Also for setting the bar for what a boss should be in my opinion.

Thank you Elisa Poletì, Chris Magazzeni, Chris Ogunlesi, Zoé Faes, Charlène Doucet, Veronica Vilona, Hammad Khan, David Vogt. It would certainly would have been more difficult for me doing this without the companionship of all of you.

Dankjewel to Nelleke Honcoop for putting up with my quirks and providing support. Dutch integration could not have been better. In the end, you still volunteered to be this thesis's spelling nazi.

Em Português,

Para todos os meus amigos que fizeram questão de me visitar durante este período quero também deixar um grande 'obrigado'! Espero ter sido o anfitrião que vocês merecem por me terem aquecido o coração com as vossas presenças.

Um especial obrigado à Nini Anes, que sempre fez tudo dentro do seu alcance para que eu estivesse o melhor possível.

Não posso deixar de reconhecer a importância que as minhas vivências académicas tiveram no meu percurso para chegar onde me encontro, bem como as pessoas que comigo as viveram na minha *Alma Mater*, FEUP. Não agradeço, mas ergo meu copo bem alto, não com alcóol, mas leite. Sei que foi graças ao eterno espírito jovem, à humildade e ao sustento para a alma que me foram dados, que aprendi a superar desafios que eu ainda nem sabia que viria encontrar. Hoje, onde quer que eu esteja, mesmo sozinho, todas as lições e experiências que tive com vós, fazem-me acreditar que vos levo comigo sempre!

Aos amigos que fiz antes de começar este trabalho deixo um forte abraço de gratidão. Ao Fernando Mouta, por sempre me mostrar o outro lado e cultivar o meu espírito crítico. Ao Tomé Duarte pela enorme inspiração que o seu carácter foi para mim, e pelo forte laço criado em tão pouco tempo. Sinto que servi contigo numa velha guerra. Ao Miguel Garcia, que sempre se preocupou que eu tivesse o futuro que eu merecia e me motivou para fazê-lo.

Uma nota especial ao Bruno Ferreira que foi meu suporte mais vezes do que ele sabe. Ao Bernardo Silva e ao João Aguiar que me ensinaram mais coisas sobre mim do que quaisquer

outras pessoas. Ao Cristhian Caldeira, que me fez uma melhor pessoa. Vós todos, meus amigos de outra vida, foram a força das minhas raízes enquanto eu tentava alcançar o céu.

Ao Pedro Marinho e ao Duarte Silva pelo seu companheirismo e forte amizade todos os dias desde que vos conheci. Cada um de nós numa cidade e sinto que estão comigo sempre para o que precisar.

Ao Pedro Aboim, meu mais antigo amigo, que sabe bem o quão este trabalho também é fruto seu também. Não tenho palavras para agradecer, mas sim esperança que saibas a eterna gratidão que sinto.

Por fim à minha família, em particular à minha Mãe, meu Pai e minha Irmã. Foram os vossos sacrifícios que me permitiram fazer tudo o que eu desejei fazer. É a vocês que dedico esta Tese, porque sei que foi o ambiente onde cresci que me moldou na pessoa que hoje sou.

Rui Feio

*“To travel any road*
*Under the sun, under the stars, nor doubt*
*If fame or fortune lie beyond the bourne -*
*Never to make a line I have not heard*
*In my own heart; yet, with all modesty*
*To say:"My soul, be satisfied with flowers,*
*With fruit, with weeds even; but gather them*
*In the one garden you may call your own."*
*So, when I win some triumph, by some chance,*
*Render no share to Caesar - in a word,*
*I am too proud to be a parasite,*
*And if my nature wants the germ that grows*
*Towering to heaven like the mountain pine,*
*Or like the oak, sheltering multitudes-*
*I stand, not high it may be - but alone!”*

Cyrano de Bergerac by Edmond Rostand
1868 – 1918

# Contents


**1 Introduction and Basic Theoretical Concepts** **1**
1.1 Introduction and Objectives . . . 1
1.2 Overview of the Work . . . 1
1.2.1 Structure . . . 2
1.3 Electromagnetic Constitutive Quantities . . . 3
1.3.1 Permittivity . . . 3
1.3.2 Permeability . . . 4
1.3.3 Refractive Index and Wave Impedance . . . 4
1.3.4 Loss Tangent . . . 4
1.3.5 Classification of materials based on electromagnetic parameters . . . 5

**2 State of the Art** **7**
2.1 Overview of Microwave Extraction Methods . . . 7
2.1.1 Measurements Setup . . . 7
2.1.2 Measurement Techniques . . . 9
2.1.3 Parameter Calculation . . . 10
2.2 Reflection only Methods . . . 11
2.2.1 Associated Issues . . . 11

**3 Analytical Model** **13**
3.1 Assumptions . . . 13
3.2 Proposed Analytical Model . . . 14
3.3 Model Imposition on the Setup . . . 18

**4 Experimental Setup and Procedure** **19**
4.1 Facilities and setup description . . . 19
4.1.1 Microwave Material RF Characterization Test Facility . . . 19
4.1.2 Submillimetre-wave Material RF Characterization Test Facility . . . 21
4.2 Measurement . . . 22
4.2.1 VNA Configuration . . . 22
4.2.2 Procedure and Known Issues . . . 23

**5 Implemented Script and Extraction Algorithm** **27**
5.1 Calibration . . . 27
5.2 Measurement Preparation . . . 29
5.3 Numerical Solver . . . 30
5.4 Initial Value Provision . . . 33
5.4.1 Seed sensitivity . . . 36

5.5 Extraction Algorithm Overview . . . . . 37
5.5.1 Model Validation with Analytical Data . . . . . 38

**6 Uncertainty Analysis** **41**
6.1 Uncertainty Budget Procedure . . . . . 41
6.1.1 Sample Thickness Variation . . . . . 42
6.1.2 Micrometer reading . . . . . 42
6.1.3 Repeatability and Reproducibility . . . . . 42
6.1.4 Software . . . . . 43
6.1.5 Temperature . . . . . 43
6.1.6 Budget . . . . . 43
6.2 Error Assessment . . . . . 45
6.2.1 Thickness Uncertainty Problem . . . . . 45
6.2.2 Facilities Comparison . . . . . 46

**7 Results** **49**
7.1 Comparison with extracted values from transmission . . . . . 49
7.2 Results Overview . . . . . 50
7.2.1 PS - Polystyrene . . . . . 50
7.2.2 PTFE -Polytetrafluoroethylene . . . . . 51
7.2.3 PEEK - Polyetheretherketon . . . . . 51
7.2.4 HF51 . . . . . 52
7.2.5 WF71 . . . . . 53
7.2.6 Comparison to Reference Values . . . . . 54

**8 Conclusion** **55**
8.1 Discussion and Conclusion . . . . . 55
8.2 Future Work . . . . . 56

**A Source Code** **57**
A.1 Source Code . . . . . 57
A.1.1 "Main" function . . . . . 57
A.1.2 "Data Reader" function . . . . . 60
A.1.3 "Calibration" function . . . . . 62
A.1.4 "Measurement Checker" function . . . . . 62
A.1.5 "Initial Value" function . . . . . 64
A.1.6 "Confirmation" function . . . . . 66
A.1.7 "Calculation" function . . . . . 67
A.1.8 "Analytical" function . . . . . 69

**References** **71**

# List of Figures


1.1 Definition of loss tangent. . . . . . . . . . . . . . . . . . . . . . . . . . . . . . 5

2.1 Different setup for free-space and transmission line methods. . . . . . . . . . . . 9

3.1 Depiction of the considered three-layer model. . . . . . . . . . . . . . . . . . . . . 14

4.1 Microwave test facility setup. . . . . . . . . . . . . . . . . . . . . . . . . . . . . . 20
4.2 High temperature sample holder setup in Microwave test facility . . . . . . . . . 20
4.3 Reflection setup in Submillimetre-wave test facility. . . . . . . . . . . . . . . . . 21
4.4 VNA time gating. . . . . . . . . . . . . . . . . . . . . . . . . . . . . . . . . . . 23
4.5 Illustration of the correction of the reference plane displacement. . . . . . . . . . 23
4.6 Holders in both facilities. . . . . . . . . . . . . . . . . . . . . . . . . . . . . . . 24

5.1 Depiction of measurements necessary for performing calibration. . . . . . . . . . 28
5.2 Effects of time-gating on extracted permittivity. . . . . . . . . . . . . . . . . . . 28
5.3 Measured S-parameters. . . . . . . . . . . . . . . . . . . . . . . . . . . . . . . . 29
5.4 Main reflection in time domain, with reference in red and with sample + reference in blue. . . . . . . . . . . . . . . . . . . . . . . . . . . . . . . . . . . . . . . 30
5.5 Real and imaginary parts of function to solve. . . . . . . . . . . . . . . . . . . . 32
5.6 3-D evolution of error function for one single frequency. . . . . . . . . . . . . . 34
5.7 Comparison between measured (thick blue) and re-constructed (thin green) S11 phase. . . . . . . . . . . . . . . . . . . . . . . . . . . . . . . . . . . . . . . . . . 35
5.8 Error between expected and calculated S11 phase over the frequency band. . . . 36
5.9 Comparison between thick and thin samples. . . . . . . . . . . . . . . . . . . . . 37
5.10 Zoom in on Error Function curves. . . . . . . . . . . . . . . . . . . . . . . . . . 37
5.11 Extracted permittivity from analytically simulated S-parameters. . . . . . . . . . 39

6.1 Thickness assessment and resulting variation in permittivity for the extreme values of thickness, where the red curve uses the maximum value and blue the minimum. 45
6.2 Assessment of the flatness of sample and its effect on permittivity. . . . . . . . . 46
6.3 Permittivity of sample taking into account the maximum and minimum deviation of thickness. . . . . . . . . . . . . . . . . . . . . . . . . . . . . . . . . . . . . . . 47
6.4 PS measured in both facilities. . . . . . . . . . . . . . . . . . . . . . . . . . . . . 47
6.5 PTFE measured in both facilities. . . . . . . . . . . . . . . . . . . . . . . . . . . 48
6.6 Repeatability with high temperature and regular setup. . . . . . . . . . . . . . . 48

7.1 PS measured in transmission and reflection. . . . . . . . . . . . . . . . . . . . . 49
7.2 PTFE measured in transmission and reflection. . . . . . . . . . . . . . . . . . . . 50
7.3 Results for PS sample. . . . . . . . . . . . . . . . . . . . . . . . . . . . . . . . . 50

7.4 Results for PTFE sample. . . . . . . . . . . . . . . . . . . . . . . . . . . . . . . 51
7.5 Results for PEEK sample. . . . . . . . . . . . . . . . . . . . . . . . . . . . . . . 52
7.6 Results for HF51 sample. . . . . . . . . . . . . . . . . . . . . . . . . . . . . . . 53
7.7 Results for WF71 sample. . . . . . . . . . . . . . . . . . . . . . . . . . . . . . . 53

# List of Tables


1.1 Classification of Material According to Electromagnetic Parameters . . . . . . . 5

4.1 Specifications of Microwave test facility . . . . . . . . . . . . . . . . . . . . . . 19
4.2 Specifications of Submillimetre-wave test facility . . . . . . . . . . . . . . . . . . 21
4.3 VNA settings used in all measurements. . . . . . . . . . . . . . . . . . . . . . . 22

5.1 Inputs of the MATLAB fucntion *fsolve* . . . . . . . . . . . . . . . . . . . . . . 31
5.2 Range of possible values assumed for the real and imaginary parts of the refractive index. . . . . . . . . . . . . . . . . . . . . . . . . . . . . . . . . . . . . . . 33
5.3 Specifications of the computer used to run developed script. . . . . . . . . . . . . 38

6.1 Uncertainty budget calculation table . . . . . . . . . . . . . . . . . . . . . . . . 43

7.1 Result of Uncertainty Analysis for PS at 33GHz. . . . . . . . . . . . . . . . . . . 51
7.2 Result of Uncertainty Analysis for PTFE at 33GHz. . . . . . . . . . . . . . . . . . 51
7.3 Result of Uncertainty Analysis for PEEK at 33GHz. . . . . . . . . . . . . . . . . . 52
7.4 Result of Uncertainty Analysis for HF51 at 33GHz. . . . . . . . . . . . . . . . . . 52
7.5 Result of Uncertainty Analysis for WF71 at 33GHz. . . . . . . . . . . . . . . . . . 53
7.6 Reference values of permittivity for tested materials. . . . . . . . . . . . . . . . . 54

# Abbreviations and Symbols

| | |
|---|---|
| 3-D | Three Dimensional |
| EM | Electromagnetic |
| ESA | European Space Agency |
| ESTEC | European Space Research and Technology Center |
| FFT | Fast Fourier Transform |
| MUT | Material Under Test |
| PEEK | Polyetheretherketon |
| PS | Polystyrene |
| PTFE | Polytetrafluoroethylene |
| RF | Radio Frequency |
| $S_{ij}$ parameters | Scattering parameters from port i to j |
| SMA | SubMiniature version A |
| TEM | Transverse Electromagnetic |
| UKAS | United Kingdom Accreditation Service |
| VNA | Vector Network Analyser |

# Chapter 1

# Introduction and Basic Theoretical Concepts

## 1.1 Introduction and Objectives

ESA/ESTEC operates some of the largest European test facilities dedicated to testing of space hardware. Among them are two RF material characterization test facilities. A submillimetre wave and a Microwave test bench. These facilities are used to provide measurement services to ESA projects and external customers and to explore and develop new measurement techniques.

In order to be able to measure some of the materials required for future ESA programs, the need of extracting constitutive material parameters has been identified. These parameters are of paramount importance for antenna design and precise knowledge of them at specific bandwidths and temperatures is required.

The development of a high temperature setup designed to characterize reflectivity losses, opened up the possibility to study the dielectric constant over a varying temperature. The setup however only allows for S11 parameters to be taken.

Another reason to further motivate S11 based methods is the fact that certain material's samples come already with an incorporated ground plane on the back, also disabling S21 measurements.

With this in mind, the development of a reflection based method for permittivity extraction in free-space was pursued.

The objective of this study is to advance the capability of the Material RF characterization test facilities at ESTEC of testing different samples and extracting the constitutive material parameters.

## 1.2 Overview of the Work

The work presented here aims to develop a new method of permittivity retrieval of materials mainly used in space applications. The technique applied only depends on reflection measurements (S11

parameters) and has no requirement of *a priori* knowledge of the dielectric constant. Precise knowledge of the thickness of the material's sample is however needed.

Three steps are required in order to perform extraction:

1. Using a VNA, measurements of the S11 parameter of a horn antenna radiating an EM wave onto a flat sample of the MUT (Material under test) are performed. The sample slab must be backed by a reference plate.

2. The ratio between the measurement with the sample in front of the reference plate, and the measurement without the sample in front of the latter, is calculated.

3. By comparison of this ratio with the expected S11 parameters computed analytically, an estimate of the permittivity is retrieved over a bandwidth.

The reference plate must also be a flat, polished metal surface that reflects virtually all of the energy impinged onto it, e.g. polished aluminium or copper. The surface of metal slab in contact with the sample serves as a reference for reflection and will be the considered the reference plane for the phase during calibration, see section 5.1.

The measurements are performed in different test benches and at different frequency bands for validation.

The final step is validation of the method by performing measurements of different materials under different environmental conditions and frequency ranges.

### 1.2.1 Structure

The work described in this document follows the following outlines:

- Chapter 1 describes the context and objectives of the proposed work, along with a brief description. It also includes an introduction to some basic theoretical concepts involved.

- Chapter 2 includes the state of the art, enumerating and describing the most widely used methods and techniques for microwave material characterization, not exclusively in free-space or using reflection measurements.

- Chapter 3 presents the chosen analytical model implemented, detailing the assumptions made and steps taken into its development.

- Chapter 4 gives out a small description of the the laboratories used for the measurements and a comprehensive explanation of the procedure followed.

- Chapter 5 focuses on the data-processing, reporting the implemented script.

- Chapter 6 includes the steps taken to calculate the associated error and the uncertainty analysis for each result.

- Chapter 7 presents the results of each material tested along with validation.

- Chapter 8 is the conclusion and offers a critical analysis of the developed work as well as a discussion of future work.

## 1.3 Electromagnetic Constitutive Quantities

Electromagnetic parameters are of paramount importance in RF engineering. These parameters define how a material interacts with surrounding electromagnetic fields, and vary widely for different materials and even under different temperatures and frequencies, in particular for space applications.

The following equations show how each parameter relate to the basic physical quantities in electromagnetism and wave propagation.

$$D = \varepsilon E \tag{1.1}$$

$D$ and $E$ are the electric displacement field and the electric field respectively. $\varepsilon$ is the permittivity.

$$B = \mu H \tag{1.2}$$

$B$ and $H$ are the magnetic field and the Magnetic field intensity. $\mu$ is the permeability.

$$J = \sigma E \tag{1.3}$$

$J$ and $E$ are the current density and the electric field. $\sigma$ is the conductivity.

### 1.3.1 Permittivity

Permittivity ($\varepsilon$), describes the interaction of a material with an electric field. This physical quantity may be expressed as a relative value between the absolute value and the permittivity of free space, and it has a complex nature with real and imaginary parts, as equation 1.4 shows. The relative permittivity may also be called dielectric constant.

$$\varepsilon_r = \frac{\varepsilon_{abs}}{\varepsilon_0} = \varepsilon_r' - j\varepsilon_r" \tag{1.4}$$

The real part, $\varepsilon_r'$ is a measure of how much energy from an external electric field is stored in the material, while the imaginary part, $\varepsilon_r$", also called the loss factor, measures how "lossy", or dissipative the material is to that same external electric field.

This parameter is also a key coefficient on the constitutive relations of the physical quantities that constitute Maxwell's equations. In equation 1.1 it is shown the relation between the electric field ($E$) and the electric flux density ($D$).

### 1.3.2 Permeability

Parallel as to what happens with the permittivity, permeability, $\mu$ has similar properties but in relation to the magnetic field instead.

$$\mu r = \frac{\mu_{abs}}{\mu_0} = \mu_r' - j\mu_r" \quad (1.5)$$

In this case, the parameter is also complex with a real part, $\mu_r'$ that is related to the stored energy in the material, when it interacts with an external magnetic field. Just as it was described in the case of the permittivity, the imaginary part, $\mu_r$" represents the energy dissipated under the same condition. In another perspective it can be seen as a measure of the ability of a material to support the formation of a magnetic field within itself.

Once again, in equation1.2 the relation between the magnetic field (H), and the magnetic flux density (B) is expressed along with its dependence on the permeability.

Concerning permeability, for non-magnetic materials the values for $\mu$ are known, i.e. equal to one.

### 1.3.3 Refractive Index and Wave Impedance

A special note must be made to mention two physical quantities because of their importance to this work. These are the refractive index, $n$ and the wave impedance, $\eta$.

Their importance resides in the fact that both are defined by the permeability and permittivity, as shown in expressions 1.6 and 1.7, and are fundamental to describe the behaviour of a travelling wave through a given medium.

The refractive index is the ratio of the velocity of light in vacuum to its velocity in a specified medium.

$$n = \sqrt{\varepsilon_r \, \mu_r} \quad (1.6)$$

The wave impedance for a TEM plane wave traveling through a given medium is equal to the intrinsic impedance of the medium.

$$\eta = \sqrt{\frac{\mu_{abs}}{\varepsilon_{abs}}} \quad (1.7)$$

The latter expression is only valid for non-conductive materials, i.e. when conductivity, $\sigma$, seen in 1.3, is equal to zero.

### 1.3.4 Loss Tangent

Another important parameter used to describe material is the loss tangent, $tan(\delta)$, sometimes called dielectric loss or dissipation factor.

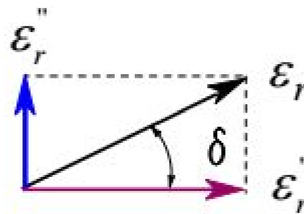


Figure 1.1: Definition of loss tangent.

To understand the meaning of this parameter we must imagine the complex value of $\varepsilon_r$ in terms of a vector in the real and imaginary axis, as pictured in figure 1.1, where its projections on each axis represent the stored and dissipated energy respectively.

Being the loss tangent the argument of the vector $\varepsilon_r$, therefore it is easy to understand why it is useful to characterize a material with this parameter, since it can tell us how much this material is lossy. The closer the value is to zero the more the imaginary value of the permittivity approaches zero and thus is less dissipative.

This is an important parameter for high frequency RF applications, where this is a driving factor for the design of high performance antennas.

### 1.3.5 Classification of materials based on electromagnetic parameters

In table 1.1 it is included a classification of materials taking into account their permittivity or conductivity. Here we can see how the complex permittivity is important to describe the nature of any given material regarding field propagation.

| $\frac{\varepsilon_r''}{\varepsilon_r'}$ | Current Conduction | Field propagation |
|---|---|---|
| 0 | - | lossless medium |
| «1 | poor conductor | low-loss medium |
| 1 | lossy conducting | lossy medium |
| »1 | good conductor | high loss medium |
| ∞ | perfect conductor | - |

Table 1.1: Classification of Material According to Electromagnetic Parameters

# Chapter 2

# State of the Art

## 2.1 Overview of Microwave Extraction Methods

Microwave methods for determining electromagnetic parameters are divided into two main methods concerning the theoretical model behind the approach. These are the resonant and non-resonant methods. Resonant methods usually have higher accuracies and sensitivities than their counterpart and can be broken down into two very general categories, i.e. resonator methods and resonant-perturbation methods, as it is further documented in [1].

The resonator method is based on the fact that the resonant frequency and quality factor of a dielectric resonator are determined by its permittivity and permeability.

Resonant-perturbation uses the change of the electromagnetic boundaries condition caused by the introduction of a sample. This perturbation also induces a deviation on the resonant frequency of the system as well as its quality factor, which once again depend on permittivity and permeability.

Non-resonant methods extract parameters based on the change of impedance that travelling waves encounter when changing media. By evaluating reflection and/or transmission of electromagnetic waves travelling through the interface of different media it is possible to deduct the permittivity and permeability of the material in question.

Since the goal of the presented work is to focus on the extraction by means of reflection measurements only, the scope of the revised literature will mostly center around non-resonant methods.

### 2.1.1 Measurements Setup

The laboratory setups used in order to acquire measurements from reflected/transmitted radiation vary significantly and all have their strengths and limitations.

The choice may depend on the nature of the MUT, such as the material's form (e.g., solid, powder, liquid, etc), size or properties (e.g., isotropic, homogeneous). The frequency of interest is also an important factor while determining the set-up technique as is the temperature at which the measurements are supposed to be performed.

Another aspect to take into consideration is if contacting or destruction of the MUT is to be avoided.

Some mainstream techniques regarding these factors will be explained in this section, referencing [2].

#### 2.1.1.1 Resonant Cavity

By connecting a resonant cavity as a sample holder to a VNA and performing readings with and without the MUT, it is possible to measure the resonant frequency and Q-factor of the cavity. From this, permittivity can be calculated with accuracy.

Although this method has a somewhat smaller bandwidth than other methods such as coaxial probe, free-space and transmission line, this specific method works best for low loss materials.

#### 2.1.1.2 Capacitance

This setup makes use of a parallel plate capacitor, with the material "sandwiched" in between and it usually uses an impedance analyzer. It is typically used at the lower frequencies, below 1 GHz and has the narrowest bandwidth of all the other setups.

#### 2.1.1.3 Coaxial probe

With the use of an open-ended coaxial probe one can measure $S_{11}$ parameters by connecting it to a port of a VNA. These reflection readings can then be expressed as a function of the medium's impedance and hence extrapolate its dielectric parameter easily.

This technique is best fit for liquids or semi-solid samples, since for solid ones a flat surface is required, as well as a thickness of at least 1 centimeter, although the theory behind it presumes an infinite thickness.

Although non-destructive and very easy to implement up to high frequencies (from 200MHz up to 50GHz), this setup is not well suited for low-loss materials or magnetic ones. It is also necessary for the material's sample to be homogeneous and isotropic.

#### 2.1.1.4 Transmission Line and Free-Space

This method can use a variety transmission “lines” to extract parameters. Lines can be coaxial, waveguide and even free-space is considered a transmission line technique.

The main advantages of free-space measurement is being non-contact and non-destructive. Preparation is also easier in comparison with some waveguide techniques. In this revision, we will focus on free-space since this will be the chosen setup for measurements.

In free-space usually horn-antennas are used to illuminate the MUT and retrieve its S-parameters. These setups can be designed for reflection or transmission measurements and can be at normal incidence or at different angles, as seen in figure 2.1.

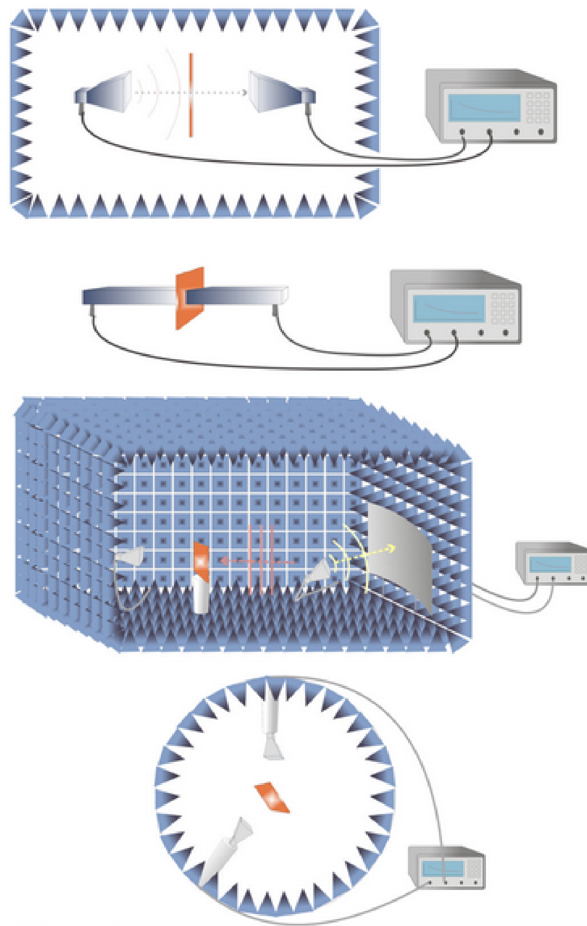

Figure 2.1: Different setup for free-space and transmission line methods.

Free-space setups allow for measurements of almost all frequency bands, provided the test bench it is equipped with the equipment for the specified band, e.g. Horn antennas, frequency extenders, VNA, etc.

Solids and thin films are usually tested in these setups.

Choosing a setup reflects on the analytical model that has to be applied later on in data processing. In the case of free-space measurements every analytical model may be decomposed into two categories, as stated in [3]. The authors propose that the several reported analytical equations that reconstruct the permittivity from measurements of the total reflection and transmission responses are equal to either the impedance method of or the propagation method, reducing every analytical method reviewed to be equivalent to one of the two models.

The impedance model is studied in different settings in [4], with special focus on reflection measurements. In the case of free-space the models treats air and sample as transmission lines with different impedance.

The propagation method is applied in [5] to describe the behaviour of S-parameters over frequency. This method usually extracts the refractive index of the material, which then can be expressed unambiguously as permittivity. This was the chosen model for the development of this work. It is noteworthy to mention that in this work the Fabry-Perot is taken into account in the model as seen in [6], where the infinite internal reflections inside a medium interfere with the measurement.

The measurement techniques used to solve the analytical models will be discussed in the next sections in regard to free-space and transmission line models.

### 2.1.2 Measurement Techniques

In literature we can find several methods to perform the measurements. The output of all of them is data that allows retrieving the material's parameter by analysis of the interaction between matter

and electromagnetic radiation.

Ellipsometry measures the change of polarization upon reflection or transmission of a wave when met with a different medium. This technique, presented in [7], [8] and [9] then uses the data of the polarization changes and compares it to a model.

Time-domain Spectroscopy is also widely used in microwave material characterization. It involves using ultra-short electromagnetic pulses and recording its temporal profile after being transmitted through [10] or reflected [11] by a given material. The authors in [12] also proposed a technique based on comparison of the measured time delay of the signal propagating through the sample, however this only works for low-loss media.

Alternatively using a network analyser to record the S-parameters of a given setup where, for instance, an antenna is radiating on a sample, provides data of the interaction between the wave and the material over a broad band. This technique also can also be used for transmission or reflection, depending on the capabilities of the setup. For most reflection setups even a one-port network analyser can be used as is in [13].

However S-parameter methods have limitations as presented in [14], as the exact same S-parameters can be obtained from very different permittivities and permeabilities. In other words there is ambiguity in the process, and if the method is not employed properly an erroneous result may be extracted. There are several ways to deal with this issue, but they will be discussed in section 2.2.1.

For this work the use of the network analyser to extract data in the frequency domain was chosen. Using this equipment with a versatile setup allows for quick measurements over entire frequency bands, as for an easy way to implement change from reflection to transmission measurements.

### 2.1.3 Parameter Calculation

Having performed measurements and chosen an analytical model to compare it with the data processing can take numerous approaches.

Iterative methods are very commonly employed to arrive at a final value for permittivity or permeability. Root-searching algorithms, such as what can be found in[15] are more resistant to uncertainty than solutions from explicit expressions, such as the one seen in [16], which is non-iterative, albeit, most of them require an initial guess of the value, a seed, in order to converge at the correct solution, as is the case in [10]. Optimization approaches are often used as well, where the aim is to minimize an error function subject to pre-determined restrains, [17].

Other interesting approaches in literature include employing genetic algorithms,[18]. This method is inspired by biological evolution, such as reproduction, mutation, recombination, and selection. Candidate solutions to the optimization problem play the role of individuals in a population.A fitness function determines the quality of the solutions and then evolution of the population takes place iteratively.

Other authors make use of graphic methods to eliminate candidates for solutions as seen in [19].

## 2.2 Reflection only Methods

Focusing on transmission line setups where S11 parameters are recorded in order to extract the sample materials, several problems arise when trying to determine the correct solution.

In the next section a final overview of the reflection only methods will be discussed, with focus on the underlying issues associated with this constraint.

### 2.2.1 Associated Issues

It is clear in literature that, in order to calculate with precision both permittivity and permeability, at least two different independent measurements are required. Independent meaning that both can be described using expressions which cannot be derived algebraically from one another. In literature, some cases will use both S11 and S21 measurements to achieve this as seen in [20].

Some authors, such as [19] and [21] propose a solution that uses two samples with different thickness, in order to get two independent measurements. However the requirement of two different samples can not always be met.

Other solutions, using only one sample include varying the distance between sample and reference plate [22], and recording independent measurements at each different short-circuit terminations.

An even more ingenious solution is placing the sample in between the short-circuit termination and a layer of a well-known material, and then switch positions between sample and known material, as presented in [13]. Instead of varying the distance between sample and short-circuit the latter appears to be more easily implemented, however both cases are designed for wave-guided setups, and a free-space equivalent could proof challenging to develop.

The usage of closed-form equations, although elegant, may present a problem. When S11 parameters approaches zero the equations may become unstable. This happens as well in the presence of resonant frequencies as studied in [23]. These frequencies occur at multiple integers of half the wavelength.

The assumption that the material is non-magnetic, $\mu = 1$, leaves us only with permittivity as a variable to determine and, in this way two independent measurements are no longer required. Nevertheless, by using S-parameters ambiguity regarding the phase, or real part, still exists, as mentioned before. In order to solve this ambiguity several solutions are found in literature, from using initial values for the iteration already very close to the correct solution, [10] or by other cross-referencing means.

The authors in [14] , propose several solutions to solve the ambiguity of S-parameters. Once again, using two different sized samples counts as one of them.

By aid of measurement performed at single frequencies one can apply the group delay method. This method proposes the calculation of the group and phase delay for two adjacent frequencies and then, assuming that the group and phase delay should be minimal, express the refractive index in terms of dispersion. The group delay method only applies for weakly dispersive media however.

The authors present one final alternative to solve ambiguity by using the Kramers-Kröng relations. The idea behind it is that the imaginary part of the refractive index is uniquely determined and can be used to reconstruct the correct value for the real part via the Kramers-Kröng relationship. This could then be used to solve ambiguity associated with the real part. The integrals involved in this method are infinite and heavy for computation but can still provide a good solution as seen in [24].

# Chapter 3

# Analytical Model

## 3.1 Assumptions

The chosen analytical model aims to describe mathematically and approximately fit the conditions of the measurements performed in the laboratory.

The following assumptions are made:

- Uniform wave incidence at normal angle;
- Material's surface to be homogeneous and flat;
- Absence of air gap between sample and metal reflector;
- Material to be isotropic and non-magnetic;
- Attenuation coefficient not considered;
- Propagation in TEM mode;

Although any model assumes a degree of simplification, effort was put into making sure that all of the parameters in the mathematical model can be measured accurately, as well as the uncertainty of the measurement. In other words, a more complex model could be implemented but the variable's associated error would not be measurable with certainty.

Let us consider for instance, a model taking into account the air gap between the sample and the metal surface. This would describe more accurately the measurement because in most cases the sample is not held in vacuum against the metal surface. Also, if the sample does not have a flat surface, the air gap can even be larger at the center of the sample. The downside of this approach is that the precise length of that space between sample and metal would be required, plus the error associated with that estimation. This reason renders it unfeasible therefore a more simple model was considered.

## 3.2 Proposed Analytical Model

The model considers propagation of an electromagnetic wave through three media as depicted in figure 3.1, where medium 1 is air, 2 is the MUT and medium 3 is a polished metal reflector surface, e.g. aluminium.

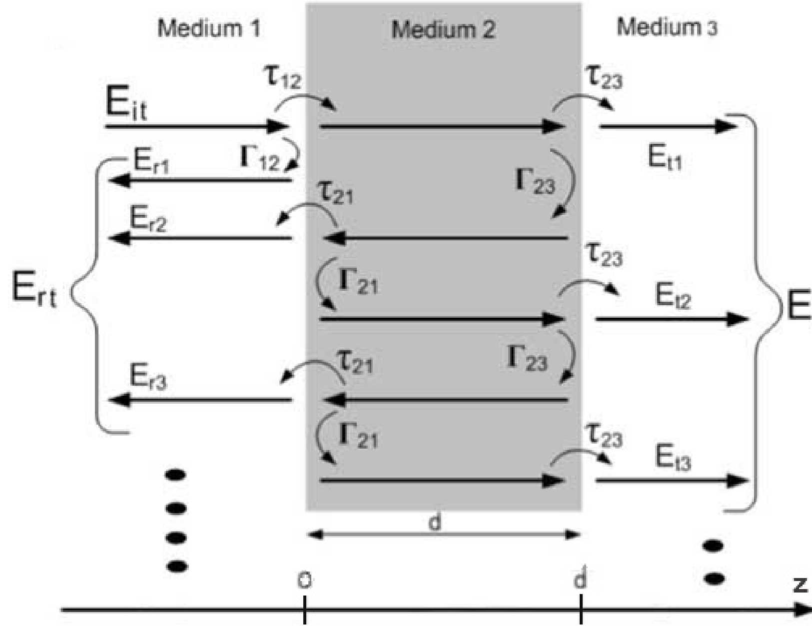


Figure 3.1: Depiction of the considered three-layer model.

$E_{it}$, $E_{rt}$ and $E_t$ are the incident, reflected and transmitted wave respectively. Regarding the developed work, the transmitted wave is null since medium 3 is a reflector plate and, for this reason it will not be considered further.

$\Gamma_{ab}$ and $\tau_{ab}$ are the reflection and transmission coefficients from medium a to b. In this case, ”a” and ”b” take the number of the medium in question, where a is the medium of origin and b is the subsequent medium.

$E_{r1}$ represents the first reflection of the incidence wave at the first interface between medium 1 and MUT, while $E_{r2}$ and $E_{r3}$ are the fractions of the waves that got reflected at the second interface (between MUT and medium 3) and went on to be transmitted back to medium 1. $E_{r2}$ and $E_{r3}$ are part of an infinite sum of reflections that occur inside the MUT and travel back to medium 1. These internal reflections are the result of the Fabry-Pérot effect.

This effect consists of multiple reflections of a wave that take place inside a medium, i.e. the MUT After being transmitted from medium 1 to 2, the wave meets the interface between media 2 and 3. At this point, a part of the power is reflected back into the MUT (by the factor of $\Gamma_{23}$) until it meets the interface between media 2 and 1 again. Here a part of the power is once again reflected back into the material, while some power is transmitted along to medium 1 by the factor of $\tau_{21}$.

This cycle repeats itself infinitely, and with each iteration power is lost in accordance to the attenuation constant and the distance it travels through the MUT.

Although in figure 3.1 only the first waves of this phenomenon are represented, the analytical model takes into account the the infinite sum of waves from $E_{r2}$ up to $E_{ri}$, assumings the attenuation is negligible due to the low loss nature of the tested materials and the relative small thickness of the materials tested.

$i$ takes the value of all the positive integers from one to infinity.

The resulting sum from $E_{r2}$ up to $E_{ri}$, along with $E_{r1}$, compose the total reflection present in medium 1, $E_r$.

The waves depicted in figure 3.1 can be written as follows:

$$E_{it} = E_i \ e^{-jk_1z} \tag{3.1}$$

$$E_{rt} = E_r \ e^{+jk_1z} \tag{3.2}$$

$$E_{r1} = \Gamma_{12} \ E_i \ e^{+jk_1z} \tag{3.3}$$

$$E_{r2} = (\tau_{12} \ \Gamma_{23} \ \tau_{21}) \ E_i \ e^{-j2k_2d} \ e^{+jk_1z} \tag{3.4}$$

$$E_{r3} = (\tau_{12} \ (\Gamma_{23})^2 \ \Gamma_{21} \ \tau_{21}) \ E_i \ e^{-j4k_2d} \ e^{+jk_1z} \tag{3.5}$$

The variable $d$ is the thickness of MUT.

It is also important to note that in this notation, the negative sign in the exponential term is conventioned to be the direction of propagation of the incident wave. $z$ is the distance travelled by the wave and it is considered that at the first interface between media 1-2, $z$ is equal to 0. At the second interface, 2-3, $z = d$.

$k_i$ is specific to the medium where propagation occurs. It is equal to the following expression, where $i$ takes the number of the medium in question:

$$k_i = \frac{w \ n_i}{c} \tag{3.6}$$

$w$ is the angular frequency in radians per second, $c$ the speed of light expressed in meters per second, and finally $n_2$ represents the refractive index of that same medium, in this case the medium is the MUT.

Now we can express $E_r$ present in medium 1 using equations 3.3 to 3.5, as the following infinite sum:

$$E_r = \Gamma_{12}\, E_i \;+\; \tau_{12}\, \Gamma_{23}\, \tau_{21}\, E_i\, e^{-j2k_2d} \Big(1 \;+\; \Gamma_{21}\, \Gamma_{23}\, e^{-j2k_2d} + (\Gamma_{21})^2\, (\Gamma_{23})^2\, e^{-j4k_2d} \;+\; ... \;+\; (\Gamma_{21})^i\, (\Gamma_{23})^i\, e^{-j2ik_2d}\Big) \tag{3.7}$$

Which in turn can be written in a more elegant way as follows:

$$E_r = \Gamma_{12}E_i + \tau_{12}\Gamma_{23}\tau_{21}E_i\, e^{-j2k_2d} \sum_{i=0}^{\infty} (\Gamma_{21}\Gamma_{23}e^{-j2k_2d})^{\,i} \tag{3.8}$$

Where the first addend is the reflection at the front of the MUT, the second is the reflection at the back of the MUT, and the infinite sum is the Fabry-Pérot effect's internal reflections.

With equation 3.8 we can now write an expression for the S11 parameter in terms of $k_2$, and as a fucntions of frequency:

$$S11(w) = \frac{E_r}{E_i}$$

$$S11(w) = \Gamma_{12} \;+\; \tau_{12}\, \Gamma_{23}\, \tau_{21}\, e^{-j2k_2d} \sum_{i=1}^{\infty} (\Gamma_{21}\, \Gamma_{23}\, e^{-j2k_2d})^{\,i}$$

$$S11(w) = \Gamma_{12} \;+\; \tau_{12}\, \Gamma_{23}\, \tau_{21}\, e^{-j2k_2d} \left(\frac{e^{j2k_2d}}{e^{j2k_2d} - \Gamma_{21}\, \Gamma_{23}}\right)$$

$$S11(w) = \frac{\Gamma_{12} \;+\; e^{-j2k_2d}\, \Gamma_{23}\, (\tau_{21}\, \tau_{12} \;-\; \Gamma_{21}\, \Gamma_{12}\,)}{1 \;-\; \Gamma_{21}\, \Gamma_{23}\, e^{-j2k_2d}} \tag{3.9}$$

The previous expression can be written in a more elegant manner if we consider that:

$$\Gamma_{ab} \;=\; -\,\Gamma_{ba} \tag{3.10}$$

$$\tau_{ab} \;=\; 1 \;+\; \Gamma_{ab} \tag{3.11}$$

With these, we can simplify the term in parenthesis of the expression in 3.9:

$$\begin{aligned}
(\tau_{21}\, \tau_{12} \;-\; \Gamma_{21}\, \Gamma_{12}\,) \;&=\; (1 \;+\; \Gamma_{21}\,)\, (1 \;+\; \Gamma_{12}\,) \;-\; \Gamma_{21}\, \Gamma_{12} \\
(\tau_{21}\, \tau_{12} \;-\; \Gamma_{21}\, \Gamma_{12}\,) \;&=\; (1 \;-\; \Gamma_{12}\,)\, (1 \;+\; \Gamma_{12}\,) \;+\; \Gamma_{12}^{\;2} \\
(\tau_{21}\, \tau_{12} \;-\; \Gamma_{21}\, \Gamma_{12}\,) \;&=\; 1 \;+\; \Gamma_{12} \;-\; \Gamma_{12} \;-\; \Gamma_{12}^{\;2} \;+\; \Gamma_{12}^{\;2} \\
(\,\tau_{21}\, \tau_{12} \;-\; \Gamma_{21}\, \Gamma_{12}\,) &=\; 1
\end{aligned} \tag{3.12}$$

Finally, with 3.12 we can rewrite 3.9 and arrive at a closed form expression that considers the total reflection of a three-layer model that takes into account the Fabry-Pérot effect:

$$S11(w) = \frac{\Gamma_{12} + \Gamma_{23}\, e^{-j2k_2 d}}{1 + \Gamma_{12}\, \Gamma_{23}\, e^{-j2k_2 d}} \tag{3.13}$$

The reflection coefficients can be expressed in terms of the wave impedance ($\eta$) of the media, a to b:

$$\Gamma_{ab} = \frac{\eta_b - \eta_a}{\eta_b + \eta_a} \tag{3.14}$$

Since the wave impedance and the refractive index ($n$) can be written in terms of permittivity ($\varepsilon$) and permeability ($\mu$), as seen in 3.15, it is possible to re-write the reflection coefficient as a function of the refractive index.

$$\begin{aligned} \eta &= \sqrt{\frac{\mu_0\, \mu_r}{\varepsilon_0\, \varepsilon_r}} \\ n &= \sqrt{\mu_r\, \varepsilon_r} \end{aligned} \tag{3.15}$$

$\mu_0$ stands for the permeability of free space. The ratio between the permeability of any given material or medium and $\mu_0$ is the relative permeability, $\mu_r$. The same relations stand for permittivity.

By rewriting 3.14 as a function of the refractive index we get 3.16, assuming that the medium in question is non-magnetic and consequently $\mu_r = 1$.

$$\Gamma_{ab} = \frac{n_a - n_b}{n_a + n_b} \tag{3.16}$$

Using the expressions in 3.16 and 3.6, we can write the expression for the S11 parameters in 3.9, as a function of the refractive index, which is the variable that we want to calculate. Considering that medium 3 is a polished metal slab and that because of this, all energy is reflected back through the medium, the value for $\Gamma_{23}$ is equal to $-1$.

$$S11(w) = \frac{\frac{n_1 - n_2}{n_1 + n_2} - e^{-\frac{j2wn_2 d}{c}}}{1 + \left(\frac{n_1 - n_2}{n_1 + n_2}\right)\left(-e^{-\frac{j2wn_2 d}{c}}\right)} \tag{3.17}$$

If we consider the complex refractive index as $n = n_r + j\,k$, where $n_r$ is the real part and $k$ is the imaginary part, the transformation from refractive index to complex relative permittivity is quite straightforward:

$$\begin{aligned} \varepsilon_{r\ real} &= n_r^2 - k^2 \\ \varepsilon_{r\ imag} &= 2\, n_r\, k \end{aligned} \tag{3.18}$$

Having arrived at a closed form expression for the S11 parameters in terms of the refractive index and angular frequency, most numerical analysis methods can be used to estimate the roots. It is of paramount importance however to note that this is an oscillating function due to its logarithmic nature, which will be plotted in figures 5.5. The non-monotonous nature of the function results in the fact that it can have different solutions. Because of this, the chosen method can diverge when trying to calculate on a solution. This problem will be discussed in detail in Chapter 5.

Performing a measurement of the S11 parameter at a single frequency point, $w$, we are left with only the refractive index of the MUT, $n_2$, as a variable. Knowledge of the MUT's thickness, $d$, is required as mentioned previously.

This analytical model, although simple, can satisfyingly describe the conditions present during a measurement of S11 parameters of a laboratory setup as depicted in figure 3.1. The validation of the model will be presented is section 5.5.1.

## 3.3 Model Imposition on the Setup

The described analytical model imposes a list of requirements of the setup as well as of the measurement procedure. This is summarized below:

- Virtually all energy must be focused at the sample;
- Reflector plate must be in held against back of the sample so that the gap in between is minimized;
- Reflector plate must be chosen so that it functions as a ground plane;
- Model assumes that S11 measurements are exclusively from the main reflection taking place at the front of the reference plate.
- Alignment of setup must be checked to ensure normal incidence.

# Chapter 4

# Experimental Setup and Procedure

For validation purposes, and to assess how reproducible the results obtained are, the measurements are performed in two different test benches over different frequency bands.

In this chapter both benches are described together with the measurement procedure necessary to each. In any one of these benches solid-state frequency extenders and mixers can be installed to perform measurement at higher bandwidths, as described in [25].

## 4.1 Facilities and setup description

### 4.1.1 Microwave Material RF Characterization Test Facility

The Microwave test facility comprises two corrugated horn antennas, one of which is mounted on a precise automated position controller, as seen in figure 4.1a. All of the axis positions can be set and consulted with a precision greater than 0.05 millimetre.

By use of collimating elliptical mirrors focused at the same position, the energy is focused towards the middle of the sample eliminating the diffraction effects of the edges of the material. Also the effect of the sample holder is minimised.

It is capable of performing material characterization of samples both in transmission and reflection concerning normal and oblique incidence.

The main parameters of this test bench are described in table 4.1. The detailed description of the test facility along with an accuracy assessment is presented in [26].

| Frequency Range (GHz): | 8 - 110 |
|---|---|
| Sample holder diameters (mm): | 400x400 and 300x300 |
| Typical edge taper over sample (dB): | -35 |
| Typical beam waist diameter (mm): | 5 $\lambda$ |
| Environment: | Anechoic Chamber |

Table 4.1: Specifications of Microwave test facility .

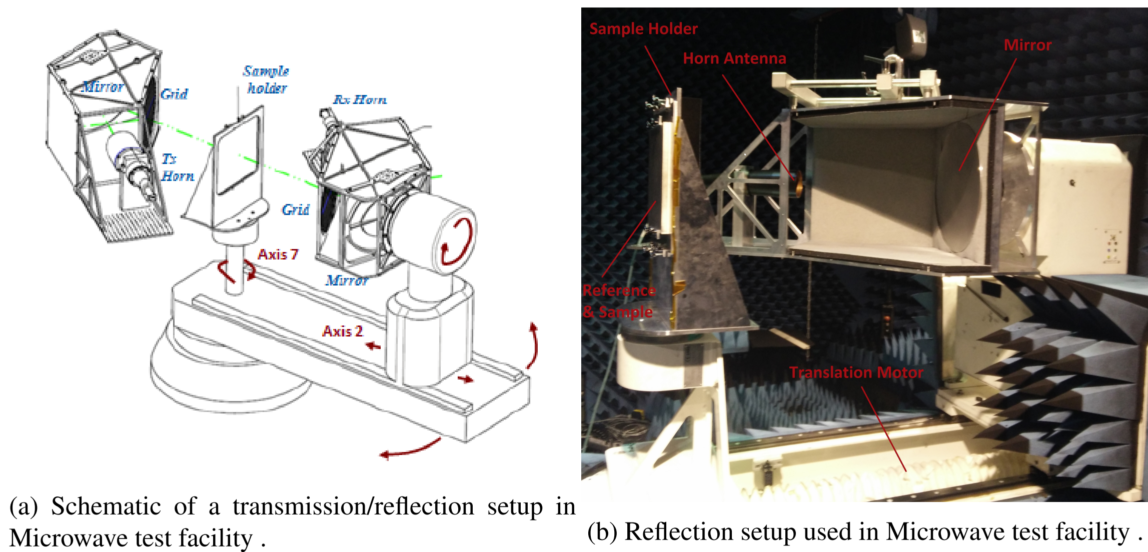


(a) Schematic of a transmission/reflection setup in Microwave test facility .

(b) Reflection setup used in Microwave test facility .

Figure 4.1: Microwave test facility setup.

In the Microwave test facility it is possible to mount a setup designed for high temperature measurements although it only offers the possibility of S11 measurements. A different sample holder is installed which, by use of a vacuum pump, holds the sample onto a copper block that can be heated up to 500° C, as seen in figure 4.2. The fixture is tested and presented in [27].

It is noteworthy to mention that this setup has the advantage of having a built-in reference metal plate that serves as holder itself, since the sample is held in vacuum on the front of the reference plate. Further discussion on this method is presented in chapter 7 where measurements of the different setups will be presented.

Figure 4.2: High temperature sample holder setup in Microwave test facility .

### 4.1.2 Submillimetre-wave Material RF Characterization Test Facility

The Submillimetre-wave test facility is a quasi-optical free-space RF measurement bench. It is also equipped with collimating mirrors but position of the feeds and sample holder is completely manual. This facility too, allows for transmission and reflection measurements in normal and oblique incidence, and is more adequate for high absorption or thick materials, in comparison to the Microwave test facility .

A description of the bench's parameters is shown in table 4.2.A more detailed description of the bench along with possible setups is referenced in [28].

| | |
|---|---|
| Frequency Range (GHz): | 50 - 750 |
| Sample holder diameters (mm): | 50, 80 and 110 |
| Typical edge taper over sample (dB): | -45 |
| Typical beam waist diameter (mm): | 45 |
| Environment: | Class 100 000 clean room area (class ISO 5 [29] ) |

Table 4.2: Specifications of Submillimetre-wave test facility .

In order to replace the ability to move the feed to a given position, a translation table was installed as part of the setup as seen in figure 4.3. Although any re-positioning is done manually, as opposed to the Microwave test facility , the relative position of the sample holder can still be measured with accuracy using a micrometer. However, only movements in the equivalent to axis 2 seen in figure 4.1a can be reproduced and measured. Rotations regarding the equivalent to axis 7 can be executed in the Submillimetre-wave test facility but with no accurate means of measuring the rotation.

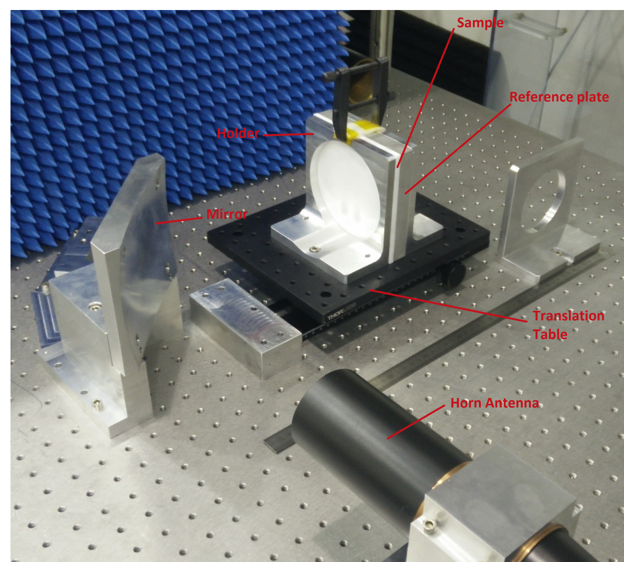


Figure 4.3: Reflection setup in Submillimetre-wave test facility.

## 4.2 Measurement

Some care must be taken into the measurement of the S11 parameters, as an inaccurate reading will result in a wrong solution for the permittivity. In this section the procedure will be described stating which steps are common to both facilities, as well as what differentiates the procedure from one test bench to the other.

Every measurement is done on a reflection setup at normal incidence, where only one feed horn is used to illuminate the area inside of the sample holder.

### 4.2.1 VNA Configuration

Throughout the measurements in both facilities the following settings on the VNA were used for S11 retrieval:

| Setting | Value |
|---|---|
| Number of points : | 2001 |
| IF Bandwidth (Hz) : | 300 |
| Time gating : | Yes |

Table 4.3: VNA settings used in all measurements.

Before proceeding to adjust the window for time gating the alignment of the setup is corrected. In the Microwave test facility the positioning of the feed and sample are automated so the direction of the wave propagation is parallel to the ground. However one must make sure the sample holder is at a normal angle of incidence, so that the assumption that all of the energy is reflected back is vlaid.

This is done by placing the reference plate at the sample holder and searching for the correct peak in the time domain, corresponding to the reflection on the plate.

Having found it, the sample holder is rotated incrementally and the amplitude is checked at each step. This rotation is done by varying axis 7 shown in figure 4.1a. When the peak is at it highest point that means we are at the optimal angle concerning the reflection of the transmitted energy. This angle is then set as a reference, to zero degrees.

In the Submillimetre-wave test facility this procedure is performed manually rotating the translation table shown in figure 4.3, since there is no motor controlling its position.

With the main reflection identified and having confirmed it at its highest magnitude value, a time gate can be applied to that pulse. Time-gating is an incorporated featured of the VNA.

This feature starts by applying a Fourier transform on the S-parameters, changing the measurement to time domain. Once in the time domain, the operator can choose the start and end point of the gate to be applied in time. This gate is a window that works similar to a band-pass filter, greatly attenuating anything outside of the defined window. This gate has a roll-off factor, therefore care should be taken when defining the edges of the gate. A too narrow gate can also attenuate a part of the lobe of interest.

Having defined the gate, changing back to frequency domain shows the S-parameters accounting for the lobe inside the time window. This greatly improves the quality of the measurement as it filters out any reflections being picked up by the feed that are not produced at the sample holder, such as reflections at the connectors or diffraction at the edges of the horn or mirror. These undesired reflections can be seen as pulses occurring at different points in the time domain, usually at lower magnitudes.

In the following pictures in figure 4.4 the main reflection pulse is depicted before and after time gated.

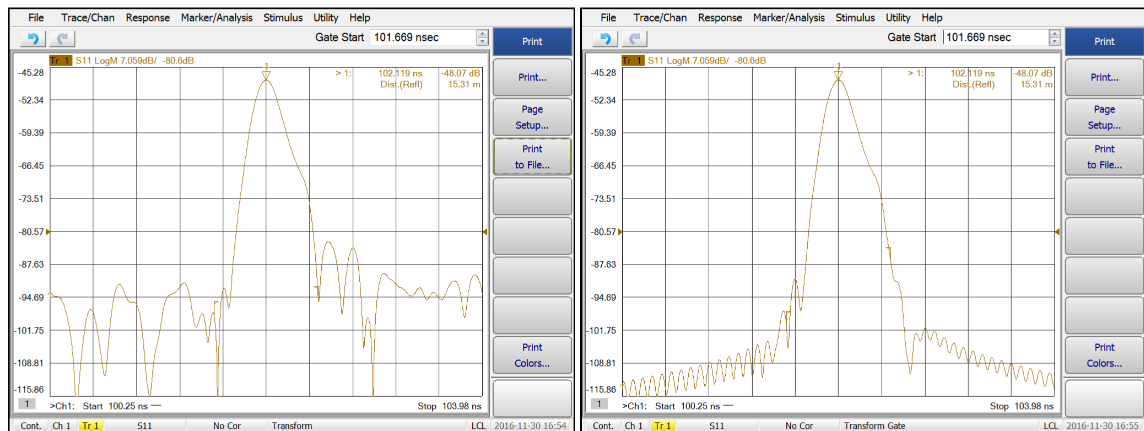


(a) Main reflection without time gating. (b) Main reflection with time gating.

Figure 4.4: VNA time gating.

### 4.2.2 Procedure and Known Issues

With the main reflection identified and time-gated it is now possible to start the measurement.

First the S11 parameters of the reference for reflection are saved. The reference plate is a high purity grade aluminium sample, machined with high precision diamond cutting and surface roughness of 50 nm rms. With this, the reference plane is defined as being the front side of the plate at the distance $L$ from the source, as shown in figure 4.5. This measurement will later be used for calibration during processing, as detailed in section 5.1.

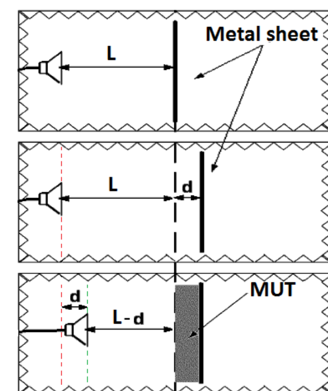


Figure 4.5: Illustration of the correction of the reference plane displacement.

To perform the same reading for the MUT it is now required to place the sample onto the holder, backing it with the same reference plate used before. This "sandwich" is clamped onto the sample holder from behind as depicted in figure 4.5. This design characteristic, present in both facilities' setups causes a shift in the reference plane equal in value to $d$, as shown in figures 4.5 and 4.6. With the sample now in place,

the reference plate has been moved away from the source by the distance equal to the sample thickness, thus changing the wave path's length.

This needs to be corrected, in order for both measurements to have exactly the same reference plane. The reference plane displacement is compensated by re-positioning the horn antenna (Microwave test facility) or the sample holder (Submillimetre-wave test facility). In the latter, re-positioning is done manually while measuring the distance of the translation table to a point of reference by aid of a caliper. In the Microwave test facility the process is completely automated. This step must be executed as accurate as possible. Intuitively, the thinner the sample and the higher the frequency, the more sensitive the extraction algorithm will be to a deviation in the reference plane's position.

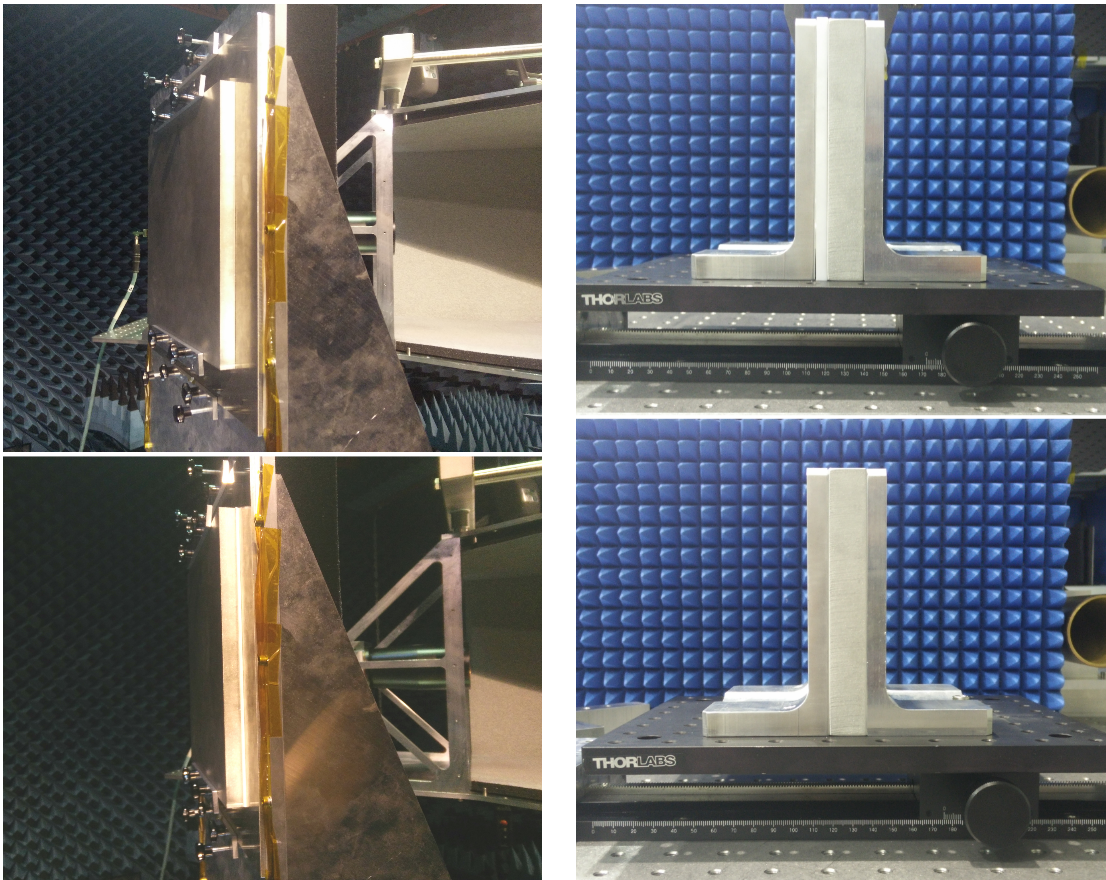


(a) Sample holder without (top) and with (bottom) sample in Microwave test facility .

(b) Sample holder with (top) and without (bottom) sample in Submillimetre-wave test facility .

Figure 4.6: Holders in both facilities.

It is also of great importance to clamp the metal sheet and sample as good as possible, in order to minimize the air gap between them and to attempt to flatten any possible curvature of the sample. The better these conditions are met, the better the measurement will fit the analytical model. Care must be taken however not to inadvertently rotate the sample holder while clamping the sample. In the Microwave test facility this setback can be checked and confirmed thanks to

the automated system. However, the same can not be checked in Submillimetre-wave test facility, without re-doing a time domain analysis by use of the VNA.

Regarding the high temperature setup in the Microwave test facility, the compensation of the reference plane shift is not necessary because the sample is held in front of the copper block, which is built in the holder. Clamping the sample is not needed since it is held in vacuum.

# Chapter 5

# Implemented Script and Extraction Algorithm

In this chapter, a detailed description of the developed script proposed to extract the permittivity of a given material is described. Intended as visual aid to this description, some figures and results are included, in order to display the algorithm's output along the process. Interpretation of this results will be reserved for discussion in greater detail in Chapter 7.

All the plots and figures displayed concern the measurement of a 5mm thick polytetrafluoroethylene (PTFE) rectangular slab with height and width of 300 millimetres, performed on a bandwidth from 27GHz to 39GHz.

The algorithm was implemented in MATLAB R2015b and the source code is included in appendix A.

## 5.1 Calibration

The measurements are performed in a controlled environment, i.e. an anechoic chamber, using a four-port VNA, although since only the S11 parameters are required, a one-port VNA would suffice.

Regarding the subject of calibration, the procedure can be divided into two different tasks. One being the calibration of the VNA itself, where there are self-calibrating techniques for one-port measurements that make use of calibration kits and are to all intents and purposes quite straightforward. In this case the only thing required of the user is to place and remove different standards as it performs an autonomous calibration.

In this section, we will focus on the second task of calibration, which is performed after measurement.

The aforementioned process requires doing a measurement first of the S11 parameters of a polished metal slab, as seen in 5.1a, taking this as the reference for reflection. This reading will be named $S11_{ref}$.

For the reference measurement, the coefficients $\Gamma_{13}$ and $\tau_{13}$, depicted in figure 5.1a, represent the reflection and transmission from media 1-3, i.e. air-metal, and hence they take the values -1 and 0 respectively, similar to what is described in Chapter 3.

Following this, another measurement is done with the M.U.T in front of the same metal slab, $S11_{samp}$ , without changing its distance from the source of radiation. The metal plate's front interface will be the reference plane, and for the calibration to be accurate this plane must not be shifted when taking both these measurements.

Taking the ratio between both these readings in the frequency domain, as seen in equation 5.1, will give the calibrated S11 parameters of the MUT.

$$S11_{cal} = -\frac{S11_{samp}}{S11_{ref}} \tag{5.1}$$

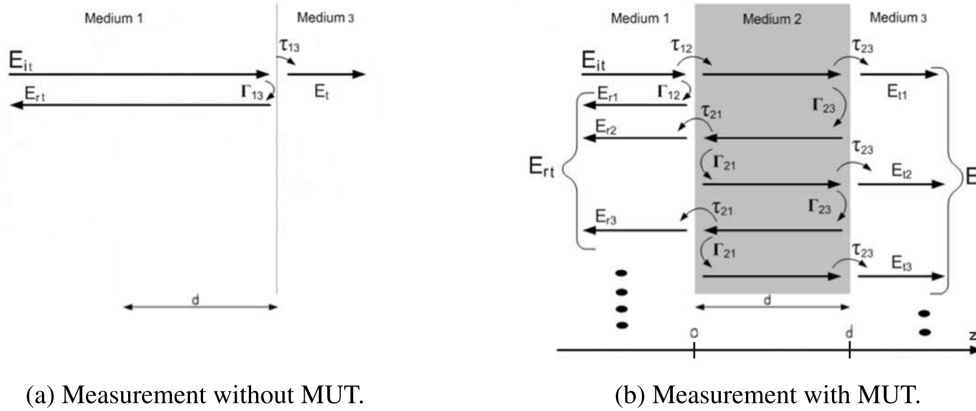


(a) Measurement without MUT. (b) Measurement with MUT.

Figure 5.1: Depiction of measurements necessary for performing calibration.

When performing calibration the script also deletes data from both measurements at the start an end of the file, corresponding to a 10% elimination of the points at the start and stop of the frequency band. This ensures that the algorithm will be fed the S11 parameters without noticeable effects of truncation due to time-gating. These effects produce erroneous values for permittivity as shown in figure 5.2, where we can see at the edges of the bandwidth the high roll-off caused.

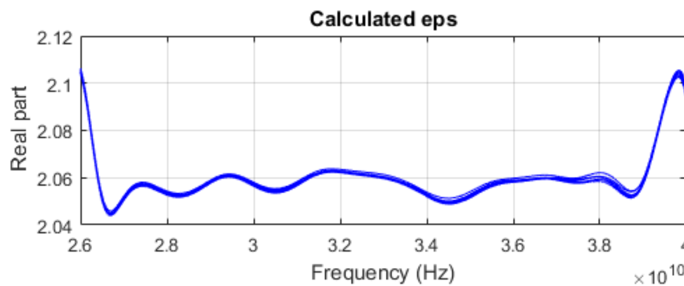


Figure 5.2: Effects of time-gating on extracted permittivity.

The before and after results of this process of elimination are shown below in figures 5.3a and 5.3b. Given that the original measurement's band is already wide enough and has enough points, the elimination of points in the files does not make a significant impact in bandwidth or resolution.

From the figure 5.3a it can be concluded that there is considerable variation (4dB) in magnitude, especially at the start of the frequency. This is exclusively an effect of time-gating and can deteriorate the quality of the measurement, as shown before in figure 5.2. The corrected S parameters are shown in 5.3b.

The top plot depicts the magnitude where the S11 parameters for both the reference and sample measurements are present. The bottom plots represent the unwrapped phase.

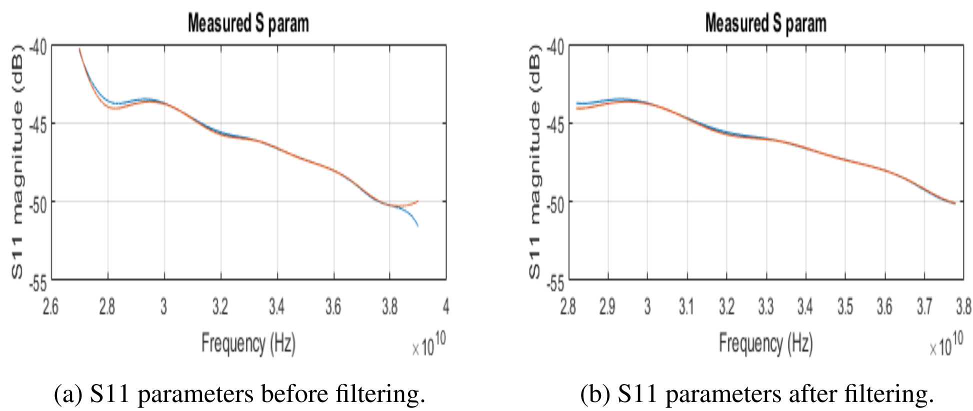


(a) S11 parameters before filtering.

(b) S11 parameters after filtering.

Figure 5.3: Measured S-parameters.

## 5.2 Measurement Preparation

As mentioned before, the reference plane must be guaranteed with accuracy to be at the same distance from the radiation source in both measurements. To confirm this, the script performs a FFT of the S parameters, thus obtaining the reflections peaks in the time domain. After this it is possible to check if the peaks occur at the same time, which implies the reference plane remains at the same distance from the feed horn.

Because of the limited resolution of the measurement performed by the VNA this step is only valid for samples that are thicker than the spatial resolution of the the reading. This resolution depends on the bandwidth and number of points used, as shown by the expression in 5.2.

$$Resolution(m) = \frac{v_{prop}}{Bandwidth} \tag{5.2}$$

$v_{prop}$ is the speed of propagation.

In other words, if the sample used is 1mm thick and the resolution is of a larger value, we cannot be sure if the reference plane is in the same positions for both readings. However, it still provides insight into the quality of the measurement in most cases.

In figure 5.4 we can see the output that the script produces after the FFT is applied. If the difference between peaks is larger than the temporal resolution then the script prompts the user with the choice to either proceed with the extraction algorithm or cancel and repeat the measurements.

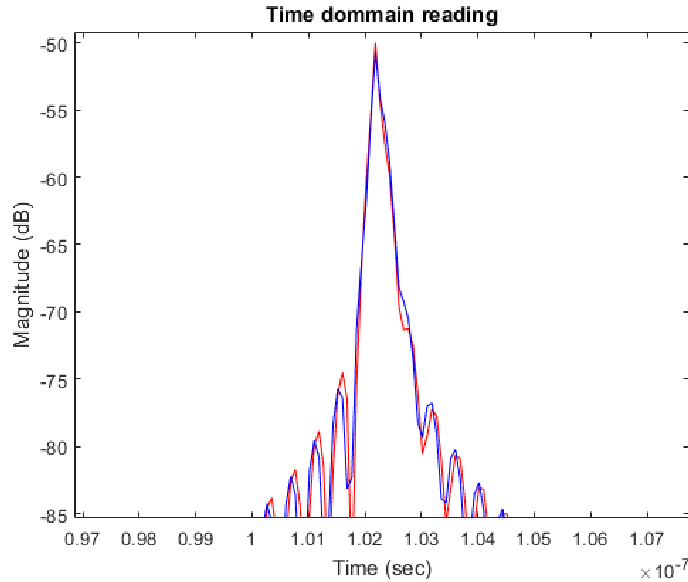


Figure 5.4: Main reflection in time domain, with reference in red and with sample + reference in blue.

## 5.3 Numerical Solver

Having the measured S11 parameters ready and an analytical expression to describe them, MATLAB provides the tools to solve the problem as long as an objective function is provided. We take the data resulting from the operation in 5.1 and subtract it to the analytical model in 3.17, which we know to accurately describe the conditions of the measurements. It is now possible to define our objective function:

$$S11_{anl} = S11_{cal} \tag{5.3}$$

Where $S11_{anl}$ is the analytical model described in chapter 3.

$$\frac{\dfrac{\frac{n_1-n_2}{n_1+n_2} - e^{-\frac{j2wn_2d}{c}}}{1+\left(\frac{n_1-n_2}{n_1+n_2}\right)\left(-e^{-\frac{j2wn_2d}{c}}\right)}}{e^{-\frac{j2wn_1d}{c}}} - S11_{cal} = 0 \tag{5.4}$$

With the equation in 5.4 finding the roots for each frequency point, $w$, leaves us with a final value for the refractive index, $n_2$.

To arrive at the roots of the expression an inbuilt MATLAB solver was employed. There are numerous numerical solvers that can be used to arrive at a solution, and MATLAB even allows

for algorithm choice in each inbuilt function. The function *fsolve* solves any system of nonlinear equations specified by $fun$, for x, where $fun$ is a function that returns a vector value, as it shown below in 5.5.

$$x = fsolve\,(fun\,,\,x0\,,\,options\,) \tag{5.5}$$

The function was applied with the following inputs presented in table 5.1. It starts at the initial value and tries to solve the equations with the optimization specified in *options*.

| Objective function ($fun$): | Expression shown 5.4 |
|---|---|
| Initial value ($x0$): | Vector described in section 5.4 |
| Options: | Algorithm: Levenberg-Marquardt |

Table 5.1: Inputs of the MATLAB fucntion $fsolve$

The Levenberg-Marquardt, [30] and [31], is based on a nonlinear least-squares algorithm. If there is no zero it still returns a point where the residual is small. However, the algorithm might converge to a point that is not a solution of the system of equations in some situations.

Like other numeric minimization algorithms, the Levenberg–Marquardt algorithm is an iterative procedure. To start a minimization, the user has to provide an initial guess for the parameter vector. In cases with multiple minima, the algorithm converges to the global minimum only if the initial guess is already somewhat close to the final solution.

As it is possible to asses from figure 5.5, where both the real and imaginary part of the function fed to the solver, there are quite a few possible solutions where the functions are equal to zero. The mesh shows the result of the function for a predefined vector of values for the real and imaginary part of the variable $n_2$.

The solver attempts to find the point where the function is equal to zero, but in this case there are multiple points that satisfy this condition. In other words, different values of $n_2$ can be used to arrive at exactly the same S-parameters.

This ambiguity in the real part of $n_2$ is what highlights the importance of the initial value being close to the correct solution. If a wrong initial value is fed into the solver it will find a root that will not be the correct solution, but still obey the function perfectly.

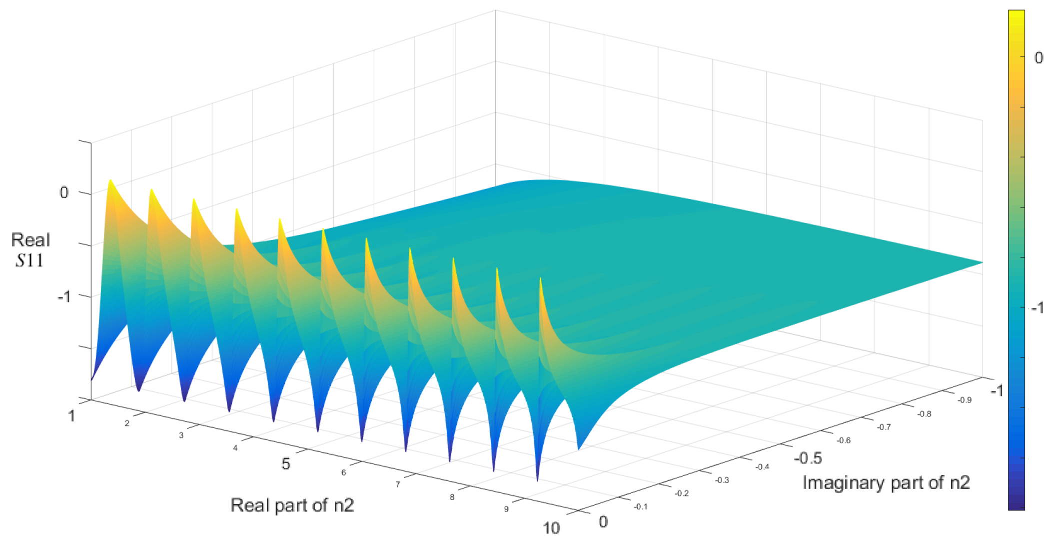


(a) Real part of function to solve.

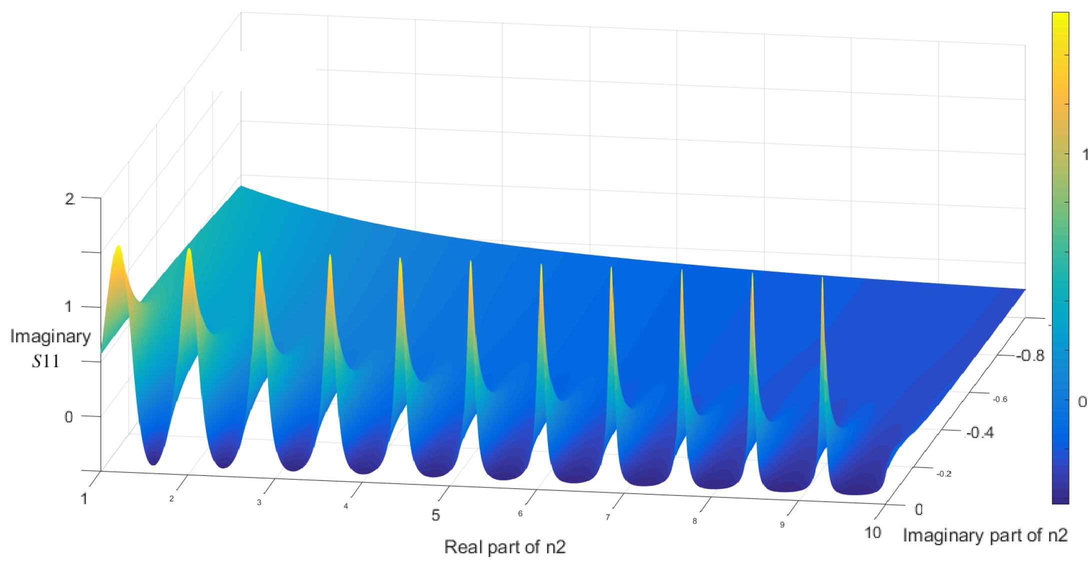


(b) Imaginary part of function to solve.

Figure 5.5: Real and imaginary parts of function to solve.

## 5.4 Initial Value Provision

Finding the roots by using the numerical solver requires an initial value that needs to be a close estimate of the solution. However, because of the periodic nature of the exponential terms present in the function in question, there are an infinite number of possible solutions that satisfy the objective function. This problem can complicate the process of choosing the initial seed that will make possible to arrive at the correct root. One approach to this problem would be for the script to require of the user some knowledge of an approximate value of the solution. However, it was decided for this work that a completely autonomous script was to be implemented, in case the properties of the MUT were completely unknown.

To estimate a seed that will produce convergence at the correct root, we begin by analysing the objective function that the solver uses. The function present in 5.3 has as variable $n_2$, the refractive index of the MUT, which can be written in the rectangular form as $n_2 = n_r + j\,k$.

We start by synthesizing two vectors composed of possible values for both the real and imaginary parts, $n_r$ and $k$, so that we can replace them in the objective function and see how the function behaves with the variation of $n_2$'s real and imaginary parts, at a specific frequency, $w$.

For this analysis to be made an error function is necessary. It was decided to use a simple error function that expresses the ratio between the measurement and the analytic function, as seen in 5.6, taken from [32]:

$$EF = tanh\left[0.1\left(1 - \frac{S11_{cal}}{S11_{anl}}\right)\right] \tag{5.6}$$

The more similar the analytical function is to the measurement, the closer to zero the error function is.

This three-dimension evolution of the error function is then computed for a specific frequency, enabling us to evaluate how the error grows with the variation in $n_r$ and $k$ terms, present in the $S11_{anl}$ function. A single frequency analysis is sufficient as it is expected of the permittivity not to deviate greatly with frequency.

The vectors used for both parts of the refractive index are displayed below. Both intervals correspond to values of permittivity that include a vast majority of materials.

| Variable | Vector start | Vector end |
|---|---|---|
| $n_r$ | 1 | 10 |
| $k$ | 0 | -1 |

Table 5.2: Range of possible values assumed for the real and imaginary parts of the refractive index.

The chosen frequency is the centre of the bandwidth by default. Unless the user specifies another or if at half the bandwidth there is a proximity to a resonant frequency. In the latter case,

the script checks if at the default frequency the thickness of the material is an integer multiple of half the wavelength. If so, it uses the frequency at $\frac{3}{4}$ of the bandwidth.

The output of this step is presented in figure 5.6.

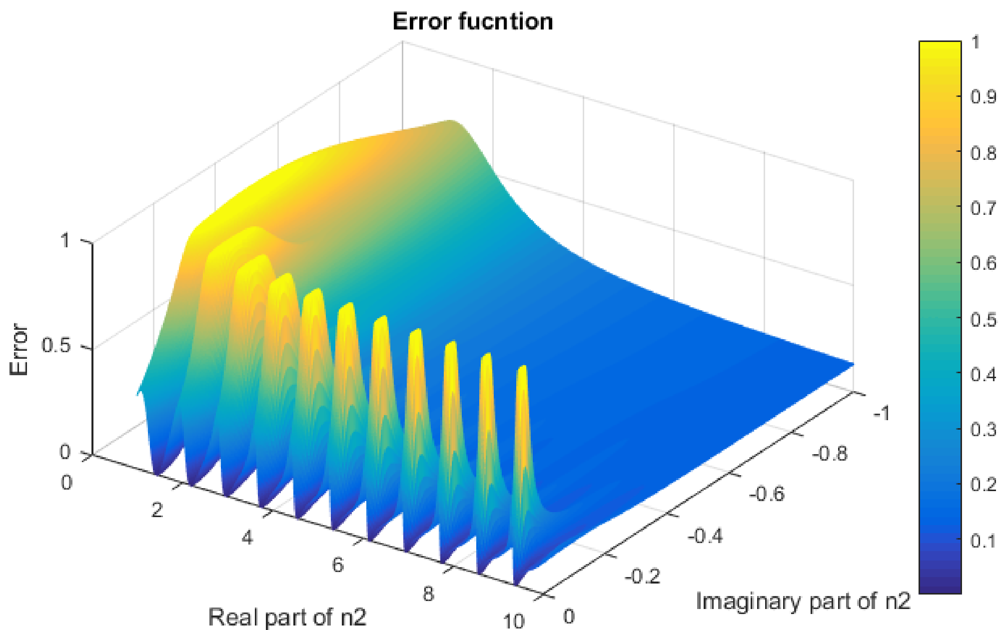


Figure 5.6: 3-D evolution of error function for one single frequency.

By examining the picture depicting the 3-D evaluation of the error function, it is easy to spot the points in space that might provide good initial estimates, although not all of them will produce the correct solution. The points where the function is of a darker shade of blue represent the lowest value of the error function. These represent values for $n_2$ where the measurement best fits the analytical model.

Each one of the points has for $xy$ coordinates, a value for the real and imaginary part of the refractive index.

Because computing the numerical solver for all the values of the entire matrix would take an exceeding amount of time, we start by eliminating points corresponding to high values of the error function, and thus cannot be a good initial seeds. For each column with the same value of $n_r$ the script returns the minimum. Following this, it goes through the aforementioned set of minima and eliminates all whose corresponding error function is greater than 0.05. This value was set as an acceptable percentage of error between model and measurement. The result are then put into a vector of possible initial seeds, which is greatly smaller than the initial matrix, and thus quicker to compute.

Having done this, we are left with a set of various possible seeds to use as initial guesses in the solver. A process is now needed to check if the result after computation of each seed is actually correct. To accomplish this, the script uses the average of the extracted permittivity to reconstruct the S11 parameters according to expression 5.3.

After completion of this process of reverse calculation, it then compares the phase of the measured S11 with the phase of the reconstructed S11 parameters throughout the full bandwidth. This comparison checks if the extracted solution, derived from a particular seed, corresponds to an S11 reading that matches the measurement.

The extraction of the permittivity, followed by the reconstruction of the S parameters and its comparison to the measurement, is performed for each value of possible seeds that are previously attained until the comparison is satisfactory.

For this comparison, the same error function as presented before is used. After having an error for each frequency point of the angle of the S parameters, the script computes the average and, if it returns a value smaller than 0.03, it considers the estimation to be successful. If this order of certainty is not achieved for any seed, it prompts the user to decide if it is preferable to repeat the process with a specified value for the average error (greater than 0.03), or abort and repeat the measurement.

The result is then presented in a plot of the superimposed phase of the S-parameters, as seen in figure 5.7. There the calibrated measurement can be seen in the thick blue trace, and the reconstructed S parameters from the average of the extracted permittivity can be seen in the thin green trace.

The discontinued blue trace is a reconstruction of phase using a previous seed, that did not satisfy comparison in order to be considered correct.

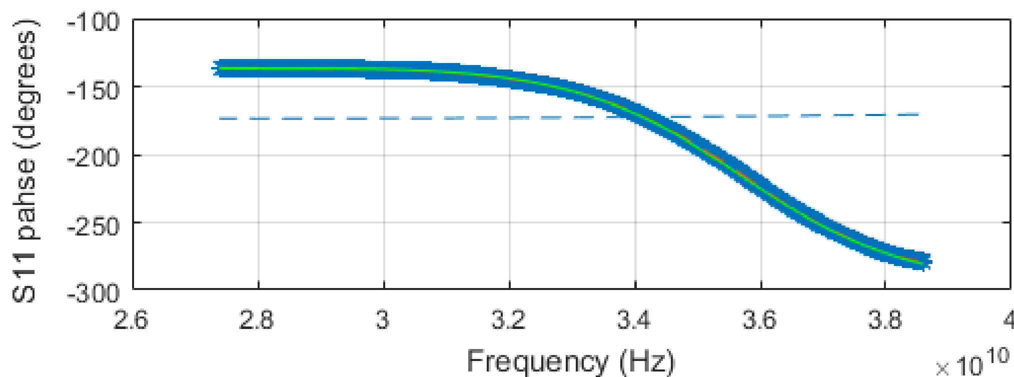


Figure 5.7: Comparison between measured (thick blue) and re-constructed (thin green) S11 phase.

Finally the script plots the real and imaginary parts of the permittivity over the bandwidth using the relation in 3.18, and the error associated with the ratio between measurement and analytical model, at each frequency point. The latter can be seen in figure 5.8.

It is important to note that the aforementioned error is derived from the error function.

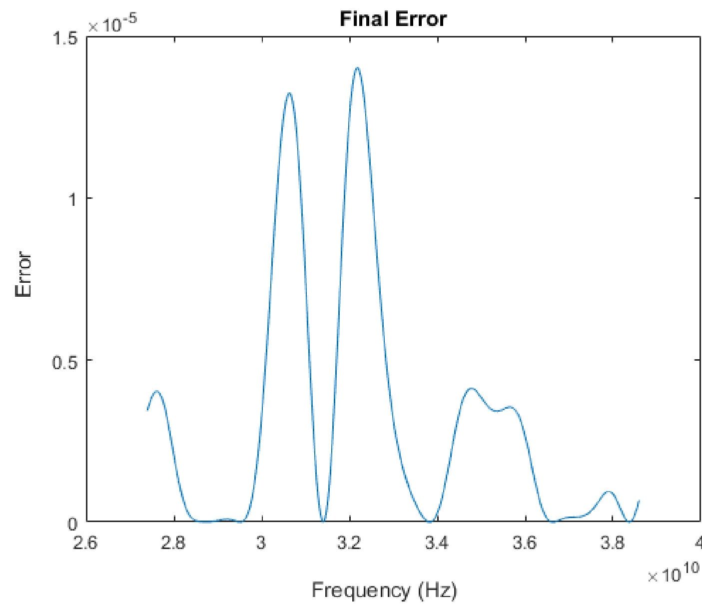


Figure 5.8: Error between expected and calculated S11 phase over the frequency band.

### 5.4.1 Seed sensitivity

In order to assess the sensitivity of the results to the seed, a simple tests was performed. In other words, it was found important to know how much could the initial value fed to the script variate and still produce the same correct result for permittivity.

To arrive at a conclusive assessment, the seed was incremented with steps of 0.05 around a center value. When the script converged to a different solution, the variation in the initial value that still would produce the same result would be known. The variation would then be expressed as a percentage of the precise value that would result in the permittivity presented in the literature or data sheet.

This small process was done for different measurements and a correlation between the seed variation and the sample thickness was established. The thinner the sample was, the more the seed could suffer a variation. It was recorded that for a sample of 0.6mm thick this variation reached 112.5%, as for a 5mm thick sample it was only 54.4%.

In figure 5.9a we see the 3-D evolution of the error function for a sample of thickness around 5mm. Next to it, in figure 5.9b, the same plot is presented but for a sample with less than a millimetre thick. By observing the curves of the surface plot, it is possible to understand the reasoning behind this fact. We can see that for the thicker sample the "valleys" are more narrow in comparison to the same curves for the thin sample.

Taking a closer look in figure 5.10 we see a zoom-in on several of these valleys with different widths. Seeing to that the script only keeps points that correspond to very dark blue regions, meaning low error, we see that the wider the "valley" is, the bigger the range of possible initials seeds, that still converge on the same value, is.

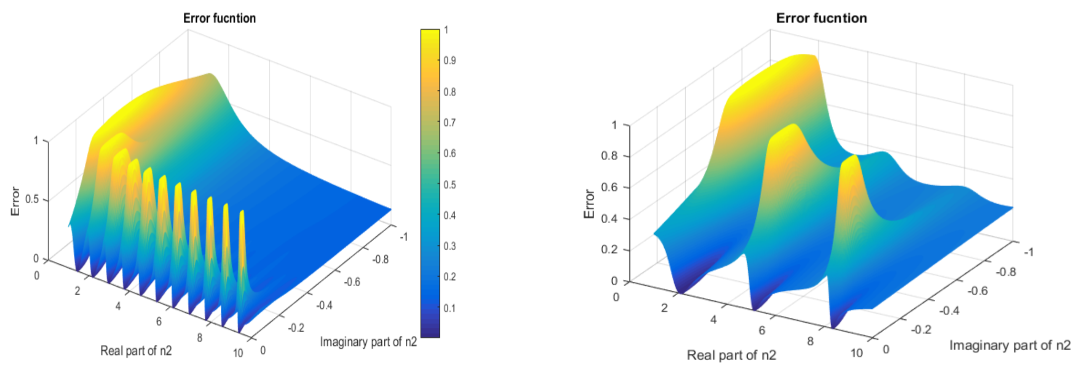


(a) 3D evolution of Error Function for thick sample. (b) 3D evolution of Error Function for thin sample.

Figure 5.9: Comparison between thick and thin samples.

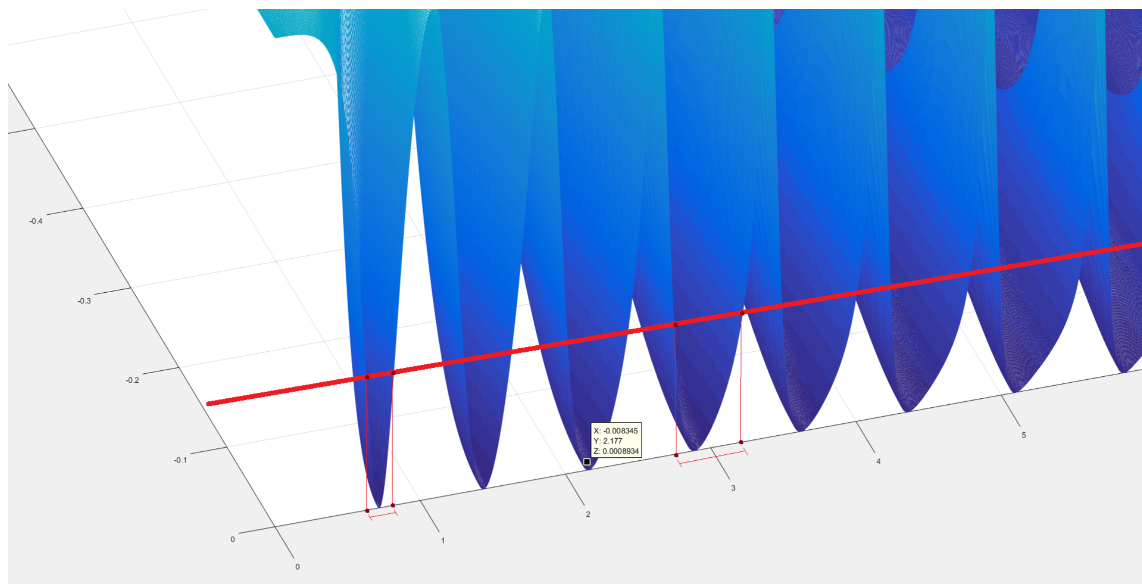


Figure 5.10: Zoom in on Error Function curves.

It is also noteworthy to mention that the higher the dielectric constant is, the more narrow these "valleys" become. Therefore it is concluded that this sensitivity to the initial value also increases with the permittivity.

## 5.5 Extraction Algorithm Overview

To summarize the extraction algorithm, we enumerate it in the following steps:

1. The 3-D evolution of the error function is computed by varying the real and imaginary part of $n_2$ at one frequency point.

2. For each set of points that share the same value of the real part $n_r$ the minimum one is kept and the rest eliminated.

3. All of the points corresponding to an error inferior to 0.05 are eliminated, resulting in the vector of possible initial values.

4. The first point of the resulting vector is used as the initial value for the numerical solver.

5. The retrieved solution is then averaged and used to reconstruct the S-parameters.

6. The reconstructed S-parameters are compared to the measurement using the error function.

7. If the error of the comparison is less than 1%, the correct solution is found. If not, step 4 to 7 are repeated using the next point of the vector of possible initial values.

The developed script takes around 24 seconds to go through one cycle of the extraction algorithm described above. This procedure is the one that contributes the most to the increase in computation time, seeing as the rest of the scrip only takes a fraction of a second.

The overall computation time depends on the value of the real part of the refraction index, since the script starts testing values at 1 and then proceeds to higher values, if a match is not found. Materials with high permittivity will take longer than those with relative lower ones.

The material's sample used as example in this chapter's figures took 25.31 seconds to arrive at a final solution. This computation was run on a computer with the following specifications:

| Processor: | Intel Core i7-3770S CPU @ 3.10 GHz |
|---|---|
| RAM memory: | 8.00 GBytes |
| System type: | 64-bit Operating System |

Table 5.3: Specifications of the computer used to run developed script.

### 5.5.1 Model Validation with Analytical Data

In order to validate the developed model and script, a simple test was performed. The script was fed with S-parameters simulated analytically using the model previously describe in Chapter 3.

Without the greater sources of uncertainties and errors involved in a real measurement, it was found that the script could return a value for the permittivity with accuracy.

By inputting a value for $n_2 = 2.05 - j0.002$ and specifying a bandwidth and thickness of sample, the script provided the permittivity with extreme accuracy, shown in figure A.1.8, thus proving the concept.

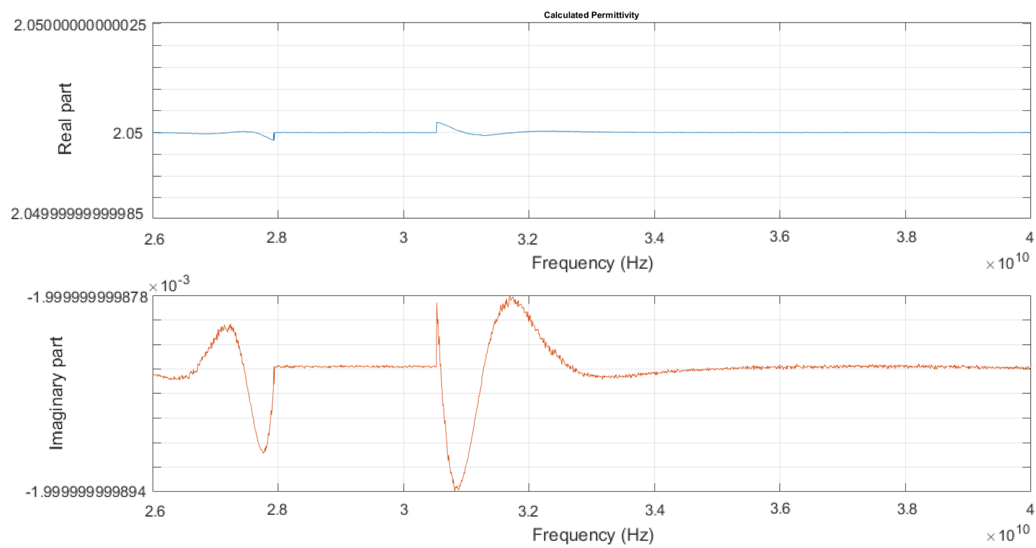


Figure 5.11: Extracted permittivity from analytically simulated S-parameters.

# Chapter 6

# Uncertainty Analysis

## 6.1 Uncertainty Budget Procedure

Every measurement has an uncertainty associated with it, unless it is an exact, counted integer, such as the number of trials performed. Every calculated result also has an uncertainty, related to the uncertainty in the measured data used to calculate it. With this in mind, any result should take into account its associated uncertainty and be expressed within a range of possible values.

To assess the uncertainty of each result a procedure was carried out in order to arrive at a confidence interval. In this section this process will be described and then applied to the materials tested.

The uncertainty evaluation of the measurements was performed in accordance with the UKAS requirements, [33], the sole national accreditation body recognised by the British government to assess the competence of organisations that provide certification, testing, inspection and calibration services. It evaluates these conformity assessment bodies and then accredits them when they are found to meet the internationally specified standard.

It is important to note that in this section, whenever error is mentioned it concerns the error associated with the uncertainty of the measurement, and is taken to be the bias from the true value. Not to be confused with the error mentioned in the error function in chapter 4, where it is simply the ratio between the measurement and the expected value derived form the analytical model.

For this evaluation the following error sources were assumed:

- The measuring instrument: Instruments can suffer from errors including bias, changes due to aging, wear, drift, electrical. noise. This is applicable to the micrometer and the VNA.
- The item being measured: The sample may not be flat or may not have a constant thickness.
- The measurement process: Throughout the measurement a small rotation of the sample holder while clamping the sample or even the clamping itself may contribute to errors.
- Operator skill: Using the micrometer requires some skill as the device needs to be perpendicular to the surface of the sample at all times.

- The environment: temperature, air pressure, humidity and many other conditions can affect the measuring instrument or the item being measured.

With this in mind, the first step is to identify measurable uncertainty parameters.

1. Sample thickness variation;
2. Micrometer reading;
3. Repeatability of S11 measurement;
4. Reproducibility of S11 measurement;
5. Software;
6. Temperature;

### 6.1.1 Sample Thickness Variation

This parameter is calculated by measuring the sample thickness a given number of times at different places using a micrometer. The mean of these readings is then calculated along with the standard deviation of the thickness and the standard deviation of the mean.

These values were calculated using expressions from 6.1 to 6.3 after eight measurements performed.

$$\overline{meas} = \frac{1}{8}\sum_{j=1}^{j=8} meas_j \tag{6.1}$$

$$s = \sqrt{\frac{1}{7}\sum_{j=1}^{j=8}\left(meas_j - \overline{meas}\right)^2} \tag{6.2}$$

$$s(\overline{meas}) = \frac{s}{\sqrt{8}} \tag{6.3}$$

### 6.1.2 Micrometer reading

This parameter is a fixed value corresponding to the mechanical uncertainty of the instrument as specified by the manual. In this case it is 0.0005 millimetres.

The micrometer used is a Mitutoyo model 293-821.

### 6.1.3 Repeatability and Reproducibility

Repeatability is calculated by measuring the S11 parameters of the reference plate eight consecutive times, while removing and placing it back in the holder. The same is then done for the sample without removing the reference plate.

This procedure is done by alternating between reading the S11 parameters of the reference plate and reading the ones from the sample, instead of performing all the eight measurements sequentially for each situation. This is done to reduce the chances of drift error in the VNA, since the calibration ratio will be using two measurements that were taken between a very small amount of time.

The same expressions seen from 6.1 to 6.3 are then applied to the calibrated S11 measurements.

Reproducibility is calculated by performing the same measurements and calculations as for repeatability but in different conditions, such as different seasons of the year or calibration settings.

### 6.1.4 Software

Given the same value for sample thickness and the same S11 measurement, the software does not appear to show any deviation.

### 6.1.5 Temperature

No impact is expected as the temperature should remain constant between the calibration and measurement itself, due to the short amount of time passed between the two.

### 6.1.6 Budget

With all the uncertainty parameters calculated, the following table, 6.1, is used to arrive at the final value of the combined standard uncertainty for each sample.

| Source of uncertainty | $s(\overline{meas})$ | Prob. Distribution | Divisor | $\delta$ |
|---|---|---|---|---|
| Sample thickness variation | | Normal | 1 | |
| Micrometer reading | 0.0005 | Rectangular | $\sqrt{3}$ | 0.00029 |
| Repeatability of S11 meas | | Normal | 1 | |
| Reproducibility of S11 meas | | Normal | 1 | |
| Combined standard deviation | - | Normal | - | |
| Expanded uncertainty (k=2.37) | - | Normal | - | |

Table 6.1: Uncertainty budget calculation table

The blank spaces on the second column of the table are filled in by the user. The values are the average for each source of uncertainty after performing eight measurements. The remainder blank spaces are the standard deviation for each source and can be filled in automatically using excel.

A divisor is used to account for the way that different probability distributions contribute different amounts to the combined uncertainty.

Uncertainties which are determined through repeated measurements are called type A, they are assumed to follow a normal distribution.

Uncertainties obtained from other means such as specifications are called type B, these may follow a rectangular distribution especially where hard limits are given for an input quantity. A rectangular distribution means that there is zero probability of the value lying outside of the limits and an equal probability of having any value within the limits. This is the case for the micrometer standard deviation.

More than two distributions of any shape will combine to give an approximately normal distribution according to the central limit theorem.

The standard uncertainty which is contributed to the combined uncertainty can be obtained by dividing the deviation by a divisor. In the case for rectangular distributions the divisor used is $\sqrt{3}$.

In order to fill in the table and arrive at a final value for the uncertainty, the following steps must be followed:

1. Calculate the average of the sample's thickness measurements.
2. Calculate the standard deviation of the mean s($\overline{meas}$) using step 1 and fill in the value for *Sample thickness variation*.
3. Divide value from step 2 by the corresponding value for *Divisor* and write it under $\delta$.
4. Calculate the average of the permittivity extracted from each S11 measurement (at a single chosen frequency).
5. Calculate the standard deviation of the mean s($\overline{meas}$) using step 4 and fill in the value for *Repeatability of S11 meas*.
6. Divide value from step 5 by the corresponding value for *Divisor* and write it under $\delta$.
7. Repeat step 4 to 6 for *Reproducibility of S11 meas*.
8. The sum of the column $\delta$ gives us the value for the *Combined standard deviation*.
9. The *Expanded uncertainty* is obtained by multiplying the value from the previous step by the *k* factor, which for this case is 2.37 in order to obtain a 95% confidence for a population of eight measurements.

The output will be the error of the permittivity that includes all the uncertainty parameters, for a specific frequency, presented as follows:

$$\overline{\varepsilon}_{@freq} \pm error \tag{6.4}$$

$\overline{\varepsilon}$ is the average of the permittivity for a single frequency and the error is the value for the expanded uncertainty.

## 6.2 Error Assessment

### 6.2.1 Thickness Uncertainty Problem

After taking into account each uncertainty parameter it became obvious that the major source of uncertainty was the thickness of the sample. In most cases, the order of magnitude of the standard deviation of the mean regarding the thickness was at least $10^2$ higher than that of the other parameters.

Considering this, and that all the micrometer readings are done at the edges of the sample, while most of the energy of the wave is focused at the center, it was decided to try and assess with precision the thickness at the center of the sample.

The result of the work done by the Metrology Section at ESTEC is presented in figure 6.1a. The sample of PTFE measured showed considerable deviation between the thickness at the edges and at the center.

Because the micrometer only allows for readings at the edges, where the sample is almost 0.2mm thicker than at the center, an erroneous assessment of the sample thickness may be fed into the script. Low uncertainty associated with the thickness measurements may not exactly mean a correct assessment of the value, due to the non-homogeneous nature of the sample.

In figure 6.1b we show how the variation of thickness present in this sample may result in a very different value for permittivity. A difference of 0.182 mm at some frequencies results in a deviation in the real part of the permittivity greater than 0.05 in permittivity.

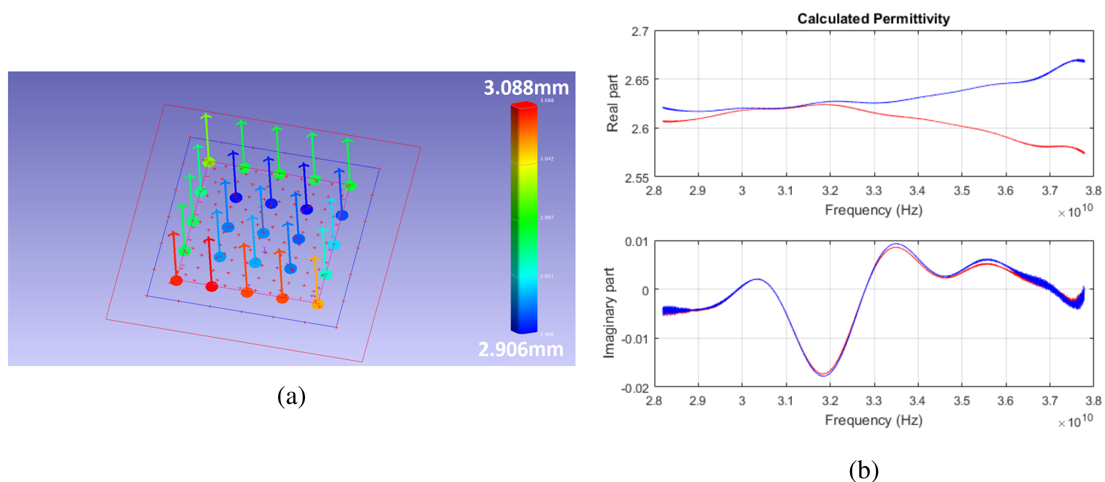


(a) (b)

Figure 6.1: Thickness assessment and resulting variation in permittivity for the extreme values of thickness, where the red curve uses the maximum value and blue the minimum.

Another source of error that could highly deteriorate a measurement is the flatness of the sample. Although, during measurements, an effort is made to keep the sample flat. If the sample is severely warped it will still show anomalies, regardless of being clamped or held in vacuum.

A curved surface on the sample will scatter the energy focused on it, and the normal incidence assumption can no longer be made. To assess how much this factor results in an incorrect result, a

flatness measurement of a somewhat bent sample was made in the Metrology section. The results are shown in figure 6.2a, where we can see that at the edges the sample has a considerably curved surface.

Using the high temperature setup and pressing the sample against the holder while being held in vacuum it was possible to flatten out the sample surface and measure the result in terms of permittivity. This measurement is compared to one done with the sample while still curved and bent in figure 6.2b. The green curve is the flatten out measurement and the red is the one done with the sample warped. We can see that a flat sample translates in a flat curve for the real part of permittivity, while a deformed one results in a wide variation.

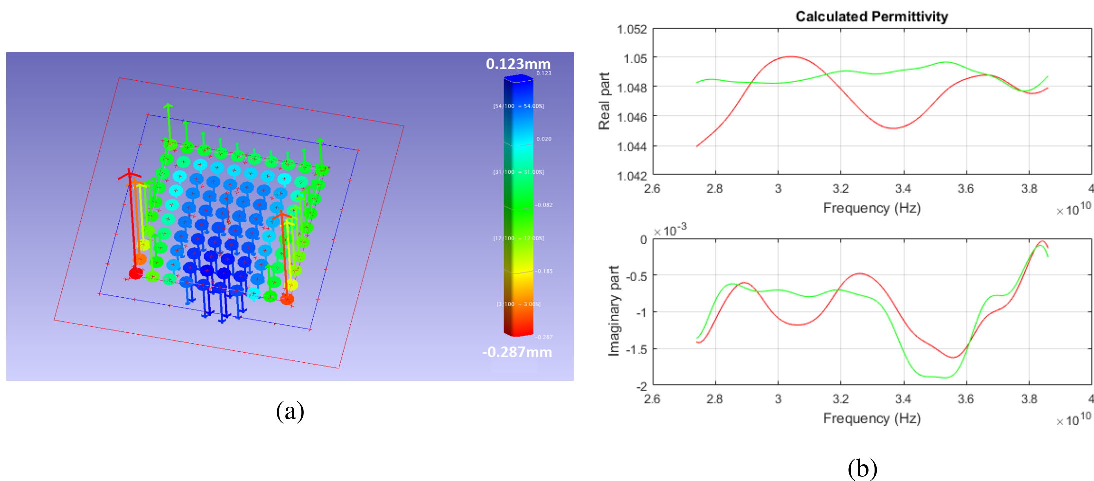


(a)

(b)

Figure 6.2: Assessment of the flatness of sample and its effect on permittivity.

The flatness analysis was inconclusive to study how flat should the sample be for accurate results. This was due to a lack of more flatness measurements.

As a final analysis on the error associated with the thickness of the sample, the maximum and minimum deviation of the average of the thickness, in this case 0.015mm, was fed into the extraction script. Since the thickness uncertainty is the major source of uncertainty, by plotting these two different curves we get the variation in permittivity associated with the thickness uncertainty, as seen in figure 6.3.The area between curves shows where the actual value for permittivity could lie, taking into account the uncertainty of the thickness measurement.

In conclusion, it was shown that the thickness measurement should have a precision of at least 0.01 millimetres at $k_a$ band. This may indicate that a good rule of thumb could be to have a thickness precision of at least two orders of magnitude smaller than the smallest wavelength, in order to achieve a precision of 0.01 in real permittivity. However, further study should be made on this.

### 6.2.2 Facilities Comparison

Finally, an assessment of the results between facilities is made. For this section, only one example is presented for a measurement performed in each bench and using the same material. The

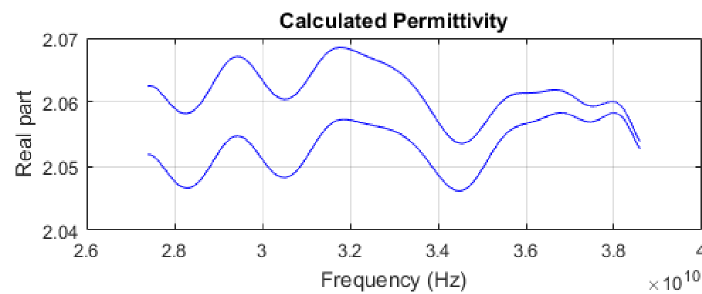


Figure 6.3: Permittivity of sample taking into account the maximum and minimum deviation of thickness.

exact same sample could not be used since the Microwave test facility and the Submillimetre test facility require different sized samples. Still, both samples come from the same manufacturer. Unfortunately, the comparison could not be done in the same frequency band.

In figure 6.4a we can see the result obtained for a PS sample in Microwave test facility, and in 6.4b, the result for PS in Submillimetre test facility. Although measurements in the same frequency band were not possible a comparison can be established bearing in mind that the real permittivity should remain flat over frequency.

In the Microwave test facility the results are slightly higher than reference values, but the flatness of the permittivity suggests the result could not be erroneous. The Submillimetre test facility measurement is within the expected.

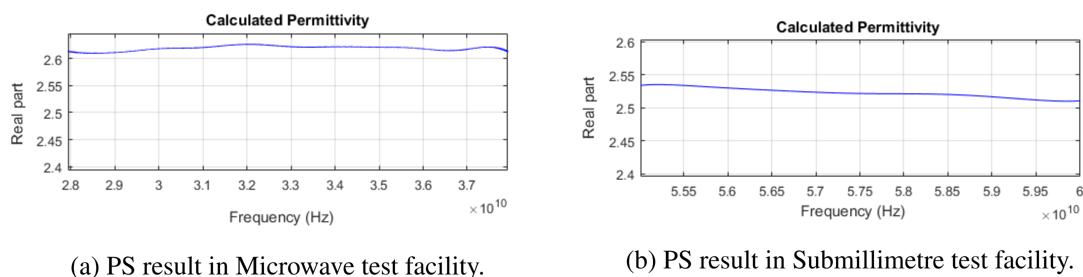


(a) PS result in Microwave test facility.

(b) PS result in Submillimetre test facility.

Figure 6.4: PS measured in both facilities.

In the next set of figures once again the facilities are compared this time using a measurement of PTFE. In figure 6.5a we see the result obtained in the Microwave test facility where the value for permittivity is acceptable. While in 6.5b, we see the same material measured in the Submillimetre test facility displays a slight curve that suggests some inaccuracy, although the range of values are also around the expected.

Although results in both facilities are very close to the expected, Microwave test facility proved to be more reliable when performing repeatability measurements.

The uncertainty in the manual positioning of the translation table in Submillimetre test facility, together with the less sophisticate clamping mechanism already described in chapter 4 , makes the Submillimetre test facility's repeatability measurements vary considerably. Also the fact that

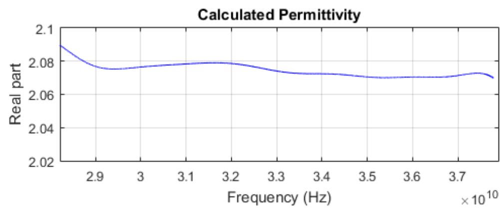


(a) PTFE result in Microwave test facility.

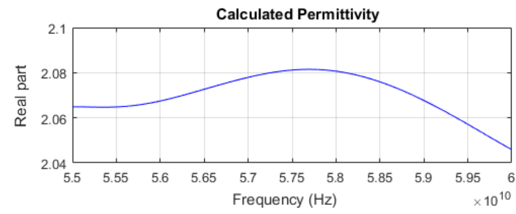


(b) PTFE result in Submillimetre test facility.

Figure 6.5: PTFE measured in both facilities.

handling the sample holder may actually rotate the table without the operator realizing it, may contribute to an augmented and considerable error. For these reasons, it was chosen to present repeatability results concerning the measurements performed in the Microwave test facility.

While performing measurements in the Microwave test facility, it was decided to compare the repeatability in both the regular setup, and the high temperature one, at room temperature. The comparison is shown in the plots of figure 6.6. We can see that the high temperature setup provided considerably more reliable results, since each measurement deviates less than those performed using the regular setup.

The reason behind this result is that for the high temperature setup, the sample is placed in front of the reference plate, without the need for any kind of reference plane shift compensation. The use of setups that require this compensation seem to introduce some inaccuracy to the final result.

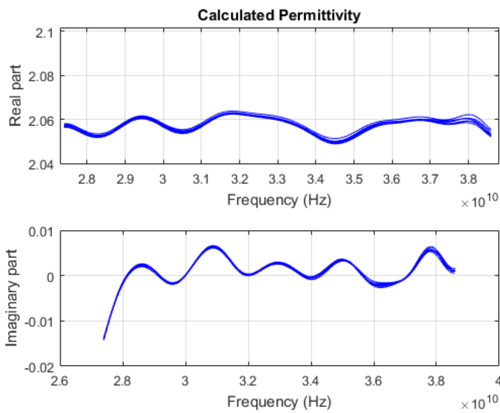


(a) Repeatability of PTFE in high temperature setup.

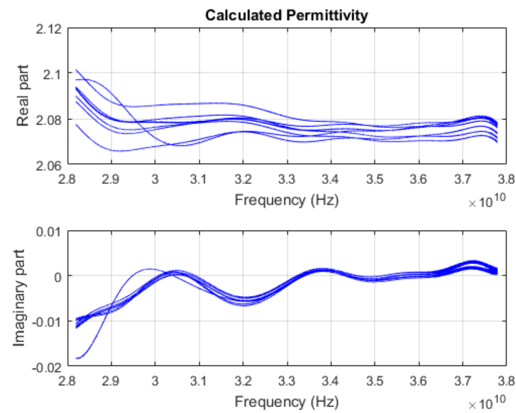


(b) Repeatability of PTFE in regular setup.

Figure 6.6: Repeatability with high temperature and regular setup.

# Chapter 7

# Results

## 7.1 Comparison with extracted values from transmission

ESTEC's Antenna section had previously characterized the material's samples in their possession using a transmission only method. Seeing to that these same samples were used to validate the reflection based method developed in the scope of this work, it would proof interesting to compare the results with the transmission results for the exact same samples.

Although not in the same frequency bands, the same samples appear to show similar values for the transmission and reflection methods, within the uncertainty of the measurement. The comparison is presented in figures 7.1 and 7.2.

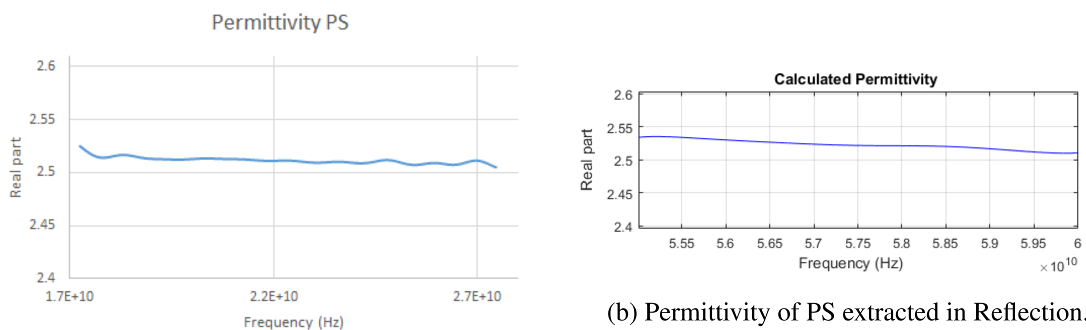


(a) Permittivity of PS extracted in Transmission.

(b) Permittivity of PS extracted in Reflection.

Figure 7.1: PS measured in transmission and reflection.

Both methods produce values that have been obtained before in literature, although for some cases, e.g. PTFE, the values shown in transmission were never reproduced in reflection. The main difference between methods resides in how much the uncertainty of the thickness measurements is a factor on the final result. In both cases, it is the major source of uncertainty, but for reflection this source has twice the impact. In other words propagation through the sample is twice as much in reflection that it is in transmission, because the wave travels through the sample in one direction and then is reflected backwards. This makes reflections measurements twice more susceptible to thickness inaccuracies when compared to transmission models.

(a) Permittivity of PTFE extracted in Transmission.

(b) Permittivity of PTFE extracted in Reflection.

Figure 7.2: PTFE measured in transmission and reflection.

## 7.2 Results Overview

In the following sections the result of the uncertainty analysis for several materials will plotted and the final value presented, taking into account the uncertainty budget. The facility that showed better repeatability results, i.e. high temperature setup, was used to extract the following results.

### 7.2.1 PS - Polystyrene

PS is a synthetic polymer used for a wide range of application. The samples used did not show any noticeable deformations, although for larger dimensions, e.g. 400 millimetre, the sample may show some surface curvature.

The result, shown in figure 7.3 and table 7.1, is well within the expected in literature, although the imaginary part shows some anomalies, since at some frequencies it takes a positive value.

(a) Extracted complex permittivity of PS.

(b) Photograph of sample of PS.

Figure 7.3: Results for PS sample.

| Mean value | ± uncertainty | Confidence Interval |
|---|---|---|
| 2.513 | ± 0.03 | 95% |

Table 7.1: Result of Uncertainty Analysis for PS at 33GHz.

### 7.2.2 PTFE -Polytetrafluoroethylene

PTFE is a synthetic fluoropolymer used in numerous applications, one being insulation in electrical wires such as SMA cables.

The result is satisfactory, although once again the imaginary part shows some anomalies, as shown in figure 7.4 and table 7.2.

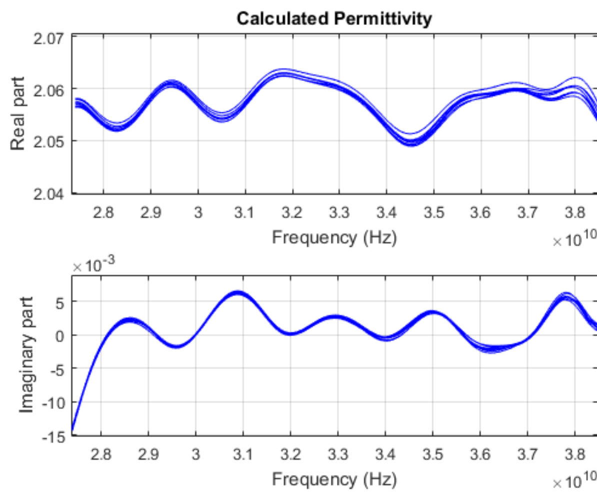


(a) Extracted complex permittivity of PTFE.

(b) Photograph of sample of PTFE.

Figure 7.4: Results for PTFE sample.

| Mean value | ± uncertainty | Confidence Interval |
|---|---|---|
| 2.060 | ± 0.0125 | 95% |

Table 7.2: Result of Uncertainty Analysis for PTFE at 33GHz.

### 7.2.3 PEEK - Polyetheretherketon

PEEK is used in navigation antennas, as well as other space applications applications. The samples used did not show any noticeable deformations.

Results, shown in figure 7.5 and table 7.3 are satisfactory but the real part should be flatter. This may be a result of poor thickness assessment.

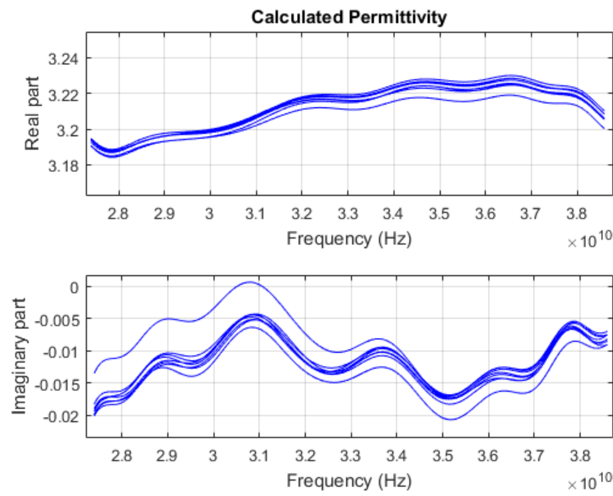


(a) Extracted complex permittivity of PEEK.

(b) Photograph of sample of PEEK.

Figure 7.5: Results for PEEK sample.

| Mean value | ± uncertainty | Confidence Interval |
|---|---|---|
| 3.217 | ± 0.0438 | 95% |

Table 7.3: Result of Uncertainty Analysis for PEEK at 33GHz.

### 7.2.4 HF51

HV51 is also used in some space applications. The nature of this material is fragile and considerably lightweight. Care must be taken while using the micrometer on the sample, because its callipers may damage the sample if too much pressure is applied.

The results were however considerably satisfactory, as can be seen in figure 7.6 and table 7.4.

| Mean value | ± uncertainty | Confidence Interval |
|---|---|---|
| 1.071 | ± 0.0075 | 95% |

Table 7.4: Result of Uncertainty Analysis for HF51 at 33GHz.

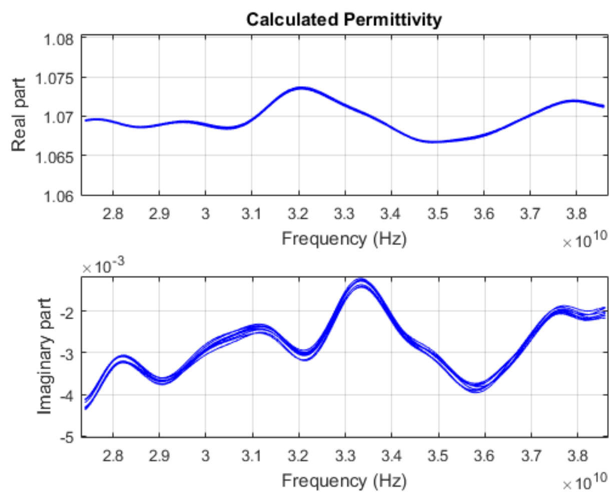


(a) Extracted complex permittivity of HF51.

(b) Photograph of sample of HF51.

Figure 7.6: Results for HF51 sample.

### 7.2.5 WF71

This sample is also very light, but stronger than HV51. Its surface however shows considerably porosity, which hindered the vacuum pump sample holder's function.

The results once again were very satisfactory as can be seen in figure 7.7 and table 7.5.

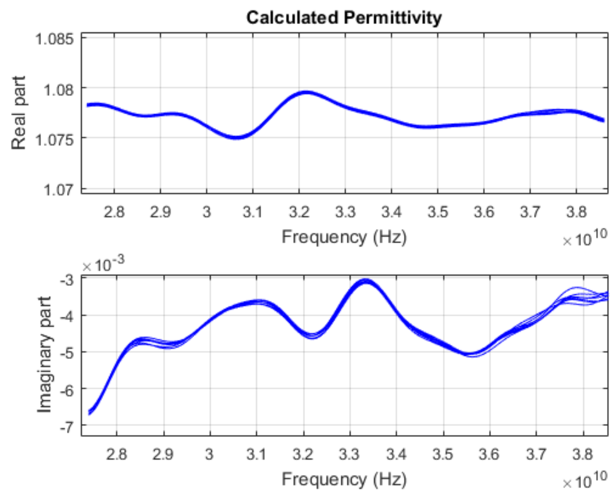


(a) Extracted complex permittivity of WF71.

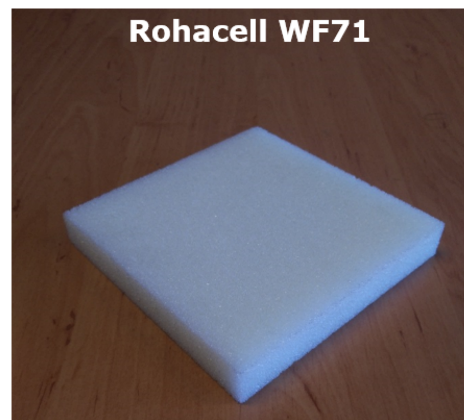


(b) Photograph of sample of WF71.

Figure 7.7: Results for WF71 sample.

| Mean value | $\pm$ uncertainty | Confidence Interval |
|---|---|---|
| 1.078 | $\pm$ 0.0559 | 95% |

Table 7.5: Result of Uncertainty Analysis for WF71 at 33GHz.

### 7.2.6 Comparison to Reference Values

Table 7.6 shows the values for the dielectric constant expected and a comparison to the extracted in the previous sections. The reference values were either taken from literature or the manufacturer's data sheet.

The frequencies and temperatures concern the referenced values.

| Material (Manufacturer) | Expected vs Extracted | Frequency (GHz) | Temperature (K) | Ref. |
|---|---|---|---|---|
| PS (Vikureen) | 2.54 vs 2.513 | 25 | 300 | [34] |
| PTFE (Vinplast) | 2.058 vs 2.06 | 35 | 300 | [34] |
| PEEK (Ketron) | 3.2 vs 3.217 | $1^{-6}$ | 293.15 | [35] |
| HV51 (Rohacell) | 1.05 vs 1.071 | 26.5 | - | [36] |
| WF71 (Rohacell) | 1.08 vs 1.078 | 26.5 | - | [36] |

Table 7.6: Reference values of permittivity for tested materials.

The anomalies present in the imaginary parts of permittivity in PS and PTFE may be a just a slight error due to extremely small order of magnitude of the value. These materials are known for their low losses, which should reflect on imaginary values very close to zero, but negative. The fact that the measurement was performed in free-space and reflection may also deteriorate accuracy in the measurement of loss.

# Chapter 8

# Conclusion

## 8.1 Discussion and Conclusion

It can be concluded that using the proposed model, and only one measurement of S11 parameters, precise knowledge of the sample thickness is required. A difference of less than a 0.2mm can result in considerable variation on the real part of the dielectric constant, depending on frequency.

Most anomalies in measurements can be attributed to the thickness assessment problem or the flatness of the sample.

Regarding the problem associated with the thickness assessment of the sample several actions can be taken to improve results.

This estimate of thickness of the MUT should be based on measurements done in the center of the sample where most energy is focused. Edges of the sample are prone to warping and may present a different value for the thickness. However, low uncertainty in measurement could still mean wrong estimation of thickness if the real part of permittivity is not a flat curve. In other words, just because repeatability seems to show a small deviation, this does not implicate a low error. Feeding a wrong value for thickness to all the measurements will result in a small deviation between permittivity, if measurements were rigorous, but the average permittivity will be a value with a large associated error. A good rule of thumb to identify this cases is to evaluate how flat the permittivity is for all repeatability measurements. The flatter it is the more close to a correct value it is.

Using smaller samples may enable thickness measurements closer to center, when using a micrometer. This may also reduce the effects of warping, seeing to that the bigger the sample is, the more susceptible to developing a curved surface it is. Using vacuum pump sample holder may enable measurement of warped samples, keeping them flat while measuring, depending on how flexible the material under test is and its thickness.

In order to improve the quality of measurements the setups should include a reliable clamping mechanism and automated positioning is an advantage when performing measurements.

If the clamping is done homogeneously over the back surface of the sample by usage of the reference plate, this could minimize the air gap between the two media and even eliminate some

curvature of the sample.

Holding samples in vacuum against the reference plate can also correct flatness and eliminate air gaps, even with more precision, but there are limitations due to the nature of the materials used. Samples that show high porosity will not hold.

Automated positioning is an excellent safeguard feature since, if the sample older is re-positioned inadvertently while performing measurements, it can be easily corrected. However, it was shown that if there is the possibility of performing measurements in a setup where the reference plate is not moved, uncertainty will be reduced considerably.

In the end, the developed algorithm was validated and it provides accurate extraction of dielectric constant using a reflection method. The script require no *a priori* knowledge of permittivity, and only one sample of the material.

Comparing the reflection method with transmission based measurements, it can be concluded that in most cases S21 parameters still produce more reliable values. This is due to the wave only travelling inside the sample half of the distance that it does in reflection, and bearing in mind that this distance is the major source of uncertainty.

## 8.2 Future Work

For a short-term future research, it would be interesting to include in the script the uncertainty analysis for several points throughout the bandwidth. This would make the extraction, with the confidence interval completely automated. It would prove useful for the degree of confidence to be a variable specified by the user.

Although the developed work provides reliable S11 parameters based values for permittivity, it was not possible apply it to high temperature measurements to see how this physical quantity variates with temperature. This however was due to setup limitations and it should prove interesting to study further as a future work. The high temperature setup was not able to hold the samples in vacuum after the heat had warped the surface of them.

For this to happen a setup where the sample can be heated while keeping its surface's shape roughly intact has to be developed. This may be challenging to develop in free-space.

Finally, using a by-static setup, where several independent readings of S11 parameters could help develop the method into one that could extract both permittivity and permeability, allowing characterization of magnetic materials.

By taking different reflection measurements of the same sample at different angles, instead of at a normal incidence, we get independent equations for the S11 parameters, which can then be used to extract both variables, permittivity and permeability, simultaneously. The analytical model should however be changed to one that takes into account polarization.

# Appendix A

# Source Code

## A.1 Source Code

### A.1.1 "Main" function

```
%%%%%%%%%%%%%%%%%%%%%%%%%%%%%%%%%%%%%%%%%%%%%%%%%%%%%%%%%%%%%%%%%%%%%%%%%%%%%%%%%%%%%%%%%%
%%
%% All copyrights regarding this source code are the intellectual property of Rui Feio.
%%
%%%%%%%%%%%%%%%%%%%%%%%%%%%%%%%%%%%%%%%%%%%%%%%%%%%%%%%%%%%%%%%%%%%%%%%%%%%%%%%%%%%%%%%%%%


function[f, eps_r, eps_i, eps, avg_err ,poss_ini] =
main(ref, samp, L, conv, mod, freq_point, tol, guess)

% ref - data from reference
% samp - data from sample
% L - thickness of sample in mm
% conv - convention of propagation exponential sign, -1 or +1
% mod - 'meas' for using real measurements or 'simu' to simulate analytical data
% freq_point - type specific freq for seed anlysys  or '[]' to use default settings
% tol - tolerance of error (e.g. 0.03)
% guess - initial value for permittivity defined by user


tic
%%%%%%%%%%%%%%%%%  INIATAILIZES CONSTANTS  %%%%%%%%%%%%%%%%%%%%%

j=sqrt(-1);
eps0 = 8.854e-12;
mu0 = 4*pi*1e-7;
c0 = 1/sqrt(mu0*eps0);
L = L*1e-3;
```

```
%%%%%%%%%%%%%%%%%%%%%%  DATA SIMULATOR  %%%%%%%%%%%%%%%%%%%%%%%

if eq(mod,'simu')

    Er = input('Type in Permittivity ( E.g.:[2.5 -0.002] )')
    freq = input('Type in frequency start and stop in GHz( E.g.:[20 40] )')
    np = input('Type in number of points ( E.g.: 2001 )')

    f=linspace(freq(1)*1e9,freq(2)*1e9,np);

    Tmeas = anl([], Er, f, L, mod, conv);

elseif eq(mod,'meas')



%%%%%%%%%%%%%%%%%%%%%%  READS FILES  %%%%%%%%%%%%%%%%%%%%%%%%%%%


[f1, S11_ref, np, BW]= data_reader(ref);
[f2, S11_samp, np, BW]= data_reader(samp);

if ne(f1,f2)
    disp('ERROR: Reference and Sample measurements are at different frequancy bands');
    pause;

elseif eq(f1,f2)
    f= f1;
end

%%%%%%%%%%%%%%%%%%%%%%  CHECKS MEASUREMENTS  %%%%%%%%%%%%%%%%%%%%%

% meas_check(S11_ref, S11_samp, np ,BW);


%%%%%%%%%%%%%%%%%%%%%%  CALIBRATION  %%%%%%%%%%%%%%%%%%%%%%%%%%%%%

Tmeas = calibration(S11_ref, S11_samp, f);
end

%%%%%%%%%%%%%%%%%%%%%%  INITIAL SEED  %%%%%%%%%%%%%%%%%%%%%%%%%%

TF = isempty(guess);

if eq(TF,1)
[EF_data,poss_ini] = seed_bourreau(Tmeas, f, L, c0, conv, freq_point);

errmin =min(EF_data(:));
```

```
end


if eq(TF,0)
    poss_ini = sqrt(guess);
end

%%%%%%%%%%%%%%%%  CALCULATION & ReCONSTRUCTION %%%%%%%%%%%%%%%%%%%%%%%




for c=1:length(poss_ini)

 [aveps ,eps, m_eps, avg_err, error, T_recons, tol] =
 conf(c, poss_ini, Tmeas, f, L, c0, conv);


if tol == 'abort'

break

end

if mean(error) < tol % if error between meas and anl is less than tolerance


eps_r = real(eps);
eps_i = imag(eps);


figure(4)
subplot(2,1,1)
plot(f, real(eps))
xlabel('Frequency (Hz)')
ylabel('Real permittivity')
hold on
grid on
title('Calculated Permittivity')
subplot(2,1,2)
plot(f, imag(eps))
ylabel('Imag permittivity')
xlabel('Frequency (Hz)')
hold on
grid on
```

```
figure(3);
subplot(2,1,1)
plot(f,20*log10(abs(T_recons)),'g')
legend('Measured Sparam')
ylabel('S11 magnitude (dB)')
xlabel('Frequency (Hz)')
title('Calibrated S param')
grid on
hold on
subplot(2,1,2)
plot(f,unwrap(angle(T_recons))*180/pi,'g')
legend('Measured Sparam')
ylabel('S11 phase (degrees)')
xlabel('Frequency (Hz)')
grid on
hold on


figure(6)
plot(f, error)
title('Final Error')
xlabel('Frequency (Hz)')
hold on

break

end



end



c


U = matlab.lang.makeUniqueStrings(samp);

T = table([f],[real(eps')],[imag(eps')]);
writetable(T ,genvarname(U));


toc


end
```

### A.1.2 "Data Reader" function

```
function [f, Sparam, np, BW , flag]= data_reader(file)

disp('Reading files:')


j=sqrt(-1);



%%%%%%%%%%%%%%%%%%%% Format Analysis %%%%%%%%%%%%%%%%%%%%%%%%%%

format = file((end-3):end); % takes last 4 characters from file name

%%%%%%%%%%%%%%%%%%%% File Reader %%%%%%%%%%%%%%%%%%%%%%%%%%

if eq(format,'.csv') % evaluates format

    header = 8;

    lines = dataread('file' ,file, '%s', 'delimiter', '\n');

    lin = length(lines) - header - 2;


    [f,S11re,S11im] = textread(file,'%f %f %f',lin,'headerlines',header,'delimiter',',');
    flag ='File read successfully';
else
    flag = 'ERROR: File format not supported';
    disp(flag);
end


%%%%%%%%%%%%%%%%%%%% Data Filtering  %%%%%%%%%%%%%%%%%%%%%%%%%%

np = length(f); % number of points
BW = (f(end) - f(1)); % bandwidth


cut = 0.1*np;
cut = round(cut);

f = f(cut:(np-cut-1)); % deletes a 10% chunk at the beggining and end of file
S11re = S11re(cut:(np-cut-1));
S11im = S11im(cut:(np-cut-1));

%%%%%%%%%%%%%%%%%%%%%%%% Plotter %%%%%%%%%%%%%%%%%%%%%%%%%%

Sparam=S11re+j*S11im; % polar form
```

```
figure(1);
subplot(2,1,1)
plot(f,20*log10(abs(Sparam)))
title('Measured S param')
xlabel('Frequency (Hz)')
ylabel('S11 magnitude')
grid on
hold on
subplot(2,1,2)
plot(f,unwrap(angle(Sparam))*180/pi)
xlabel('Frequency (Hz)')
ylabel('S11 phase')
grid on
hold on


disp(flag);
```

### A.1.3 "Calibration" function

```
function[Tmeas] = calibration(ref, samp,f)

disp('Calibrating measurements')

Tmeas = -samp./ref;

figure(3);
subplot(2,1,1)
plot(f,20*log10(abs(Tmeas)),'*')
title('Calibrated S param')
grid on
hold on
subplot(2,1,2)
plot(f,unwrap(angle(Tmeas))*180/pi,'*')
grid on
hold on
```

### A.1.4 "Measurement Checker" function

```
function []= meas_check(ref, samp, np, BW)

disp('Checking validity of measurements:')


%%%%%%%%%%%%%%%%%%%% Transform to time domain %%%%%%%%%%%%%%%%%%%%%%%%%
```

```
t_ref = ifft(ref, np);
t_samp = ifft(samp, np);

t_span = (np -1)/BW; %range in seconds

t=linspace(0, t_span, np);

dB_ref = 20*log10(abs(t_ref));
dB_samp = 20*log10(abs(t_samp));

figure(2)

plot(t, dB_ref, 'r')
title('Time dommain reading');
hold on
indexmax = find(max(dB_ref) == dB_ref);
ref_time_max = t(indexmax);

plot(t, dB_samp, 'b')
hold on
indexmax = find(max(dB_samp) == dB_samp);
samp_time_max = t(indexmax);

delta = samp_time_max - ref_time_max; % delta between peaks of reference and sample

tol = 0.5e-9; %tolerance of delta


%%%%%%%%%%%%%%%%% Reference shift checker  %%%%%%%%%%%%%%%%%%%%%

if (abs(delta) == 0)

    disp('Plane of reference shift compensated')

elseif (abs(delta) ~= 0)

    disp('WARNING: Plane of reference shift may not be accurately compensated')

    if le(abs(delta), tol)

        disp('Plane of reference shift acceptable')

    else

        disp('ERROR: Plane of reference shift not compensated')
        disp('Press any key to continue anyway')
        pause;
    end
```

```
end
```

### A.1.5 "Initial Value" function

```
function[m, poss_ini] = seed_bourreau(Tmeas, f, L, c0, conv, freq_point)

disp('Determening Initial value...')

w= 2*pi*f;
j=sqrt(-1);

%%%%%%%%%%%%%%%%%%%%%%%%%%% 3D Analysis %%%%%%%%%%%%%%%%%%%%%%%%%%

n=linspace(1,10,length(f));
k=linspace(0,-1,length(f));


alpha = 0.1; %adjustment

TF = isempty(freq_point);

if eq(TF,1)
       fp = f(((end-1)/2));
elseif eq(TF,0)
    fp = freq_point*1e9;
end


lambda_reson = ((3*1e8./fp)/2)*1e-3 ;%resonant wavelenght for thickness in mm


div = ~mod(lambda_reson/L,1); %checks resonance

if eq(div,1)
    disp('Chosen frequency is resonant!!!')

    fp = (f(((end-1)/2))) + ((f(((end-1)/2)))/2); %uses freq. point at 3/4 of the band

end


disp('Frequcny point used for seed:')

fp
```

```
for kk=1:length(f) %adjust mid frequancy point or maybe do with 2 points 35GHz

    for nn=1:length(f)

        Tcalc(nn,kk) =(((((1-(n(nn) + j*k(kk)))./(1+(n(nn) + j*k(kk))))+
        (-1).*exp((conv)*j*2*(n(nn) + j*k(kk))*(2*pi*(f(((end-1)/2)))*L/c0)))
        ./(1+((1-(n(nn) + j*k(kk)))./(1+(n(nn) + j*k(kk)))).*(-1).*exp((conv)
        *j*2*(n(nn) + j*k(kk))*(2*pi*(f(((end-1)/2)))*L/c0)))))./(exp((conv)
        *j*2*(2*pi*(f(((end-1)/2)))*L/c0))));


        EF(nn,kk) = tanh(alpha.*abs(1-((Tmeas(((end-1)/2)))./(Tcalc(nn,kk)))).^2);

    end



end
figure(1000)
mesh(k,n,EF)
zlabel('Error')
ylabel('Real part of n2')
xlabel('Imag part of n2')

savefig('Amb.fig');

h = gcf; %current figure handle
axesObjs = get(h, 'Children');  %axes handles
dataObjs = get(axesObjs, 'Children'); %handles to low-level graphics objects in axes
objTypes = get(dataObjs, 'Type');  %type of low-level graphics object

k_data = get(dataObjs, 'XData');  %data from low-level grahics objects
n_data = get(dataObjs, 'YData');
EF_data = get(dataObjs, 'ZData');

inv = EF_data';
[m, index] = (min(inv)); %returns min of each row of EF_data and its col

ii=1;
count = 0;
for i=1:length(m)

    if lt(m(i),0.01) %condition working

            possini(i) = n_data(i) + j.*k_data(index(ii));
            ii = ii + 1;
```

```
    else if ge(m(i),0.05)
            count = count+1;
        end
    end
end


poss_ini = possini(possini~=0);
```

### A.1.6 "Confirmation" function

```
function[aveps ,eps, m_eps, avg_err, error, T_recons, tol] =
conf(c,poss_ini, Tmeas, f, L, c0, conv)

tol=0.01;

seed(c) = poss_ini(c);


disp('Iteration no:')
c
disp('Seed value:')
poss_ini(c)

for i=1:length(f)

    ini(i) = seed(c);

end


[n , aveps ,eps, m_eps] = calc(Tmeas, ini, f, L, c0, conv);

%%%%%%%%%%%%%%%%%%%%%%  CONFIRMATION  %%%%%%%%%%%%%%%%%%%%%%%%%%%%%


av_n = mean(n);

for i=1:length(f)
    n_rec(i) =av_n;
end

disp('Reconstructing and comparing Sparam')


T_recons = anl(n_rec,[], f, L, 'meas', conv);
```

```
error = tanh(0.1.*abs(1-((angle(Tmeas)')./(angle(T_recons)))).^2);

disp('Error of reconstruction (%):')
mean(error)*100


avg_err(c) = mean(error)*100

if (c == (length(poss_ini))-2)
    disp('FAILURE: No result within tolerance of error')
    tol = 'abort';
  end
```

### A.1.7 "Calculation" function

```
function[n , aveps, eps, m_eps] = calc(Tmeas, ini, f, L, c0, conv)

disp('Apllying seed to Numerical approximation')

disp('Calculating final solution...')


w= 2*pi*f;
j=sqrt(-1);

%%%%%%%%%%%%%%%%%%%%%%%%%%% Solver point-by-point %%%%%%%%%%%%%%%%%%%%%%%%%%

for ff=1:length(f)

    olc(ff)=w(ff)*L/c0;

    eqn =  @(xy) (((((1-xy)./(1+xy))+(-1).*exp((conv)*j*2*xy*olc(ff)))./(1+((1-xy)
    ./(1+xy)).*(-1).*exp((conv)*j*2*xy*olc(ff)))))./(exp((conv)*j*2*olc(ff))))
    - (Tmeas(ff));


    options=optimset('Display','off', 'Algorithm','levenberg-marquardt',
    'Tolx', 1e-9 ,'Tolfun', 1e-9 );

    [n(ff),fval,exitflag,output] = fsolve(eqn, ini(ff), options);


end
```

```
%%%%%%%%%%%%%%%%%%%%%%%% Solver Flag %%%%%%%%%%%%%%%%%%%%%

if eq(exitflag,1)
    disp('Equation solved. First-order optimality is small.')
elseif eq(exitflag,2)
    disp('Equation solved. Change in x smaller than the specified tol')
elseif eq(exitflag,3)
    disp('Equation solved. Change in residual smaller than the specified tol')
elseif eq(exitflag,4)
    disp('Equation solved. Magnitude of search direction smaller than specified tol')
elseif eq(exitflag,0)
    disp('Number of iterations or function evaluations exceeded.')
elseif eq(exitflag,-1)
    disp('Output function or plot function stopped the algorithm')
elseif eq(exitflag,-2)
    disp('Equation not solved.')
elseif eq(exitflag,-3)
    disp('Equation not solved.')
end


%%%%%%%%%%%%%%%%%%%%%% Permitivitty Calc %%%%%%%%%%%%%%%%%%%%%%

nr = real(n);
ni = imag(n);

eps=n.^2;
eps_r = nr.^2-ni.^2;
eps_i=2.*nr.*ni;


%%%%%%%%%%%%%%%%%%%%%%% Average Permitivitty %%%%%%%%%%%%%%%%%%%

aveps=sum(eps_r)/length(eps_r);

for c=1:length(Tmeas)

    avge(c) = aveps;

end



m_eps = mode(eps);
disp('Average Permittivity:');
disp(aveps);
```

```
disp('Mode of Permittivity:');
disp(mode(eps))
```

### A.1.8 "Analytical" function

```
function[T] = anl(n, Er, f, L, mod, conv)


j=sqrt(-1);
eps0 = 8.854e-12;
mu0 = 4*pi*1e-7;
c0 = 1/sqrt(mu0*eps0);
w = 2*pi*f;


if eq(mod, 'meas')

    disp('Re-constructing S param')


        for ff=1:length(f)

            olc(ff)=w(ff)*L/c0;

            Tconf(ff) = ((((((1-(n(ff)))./(1+(n(ff))))+(-1).*exp(-j*2*(n(ff))*
            olc(ff)))./(1+((1-(n(ff)))./(1+(n(ff)))).*(-1).*exp(-j*2*(n(ff))*
            olc(ff))))./(exp(-j*2*olc(ff))));

            T(ff) = Tconf(ff);

end

    elseif eq(mod,'simu')

        disp('Synthetizing S param')


        E = Er(1)+j*Er(2);

        n2 = [(sqrt((abs(E)+real(E))/2)) (sqrt((abs(E)-real(E))/2))];

        for ff=1:length(f)

            olc(ff)=w(ff)*L/c0;

            Tanl(ff) = (((((1-(n2(1)-j*n2(2)))./(1+(n2(1)-j*n2(2))))+(-1).*
            exp(-j*2*(n2(1)-j*n2(2))*olc(ff)))./(1+((1-(n2(1)-j*n2(2)))./
            (1+(n2(1)-j*n2(2)))).*(-1).*exp(-j*2*(n2(1)-j*n2(2))*
```

```
            olc(ff)))./(exp(-j*2*olc(ff))));

            T(ff) = Tanl(ff);

        end

end



figure(3)
subplot(2,1,1)
plot(f,20*log10(abs(T)),'--')
title('S param')
grid on
hold on
subplot(2,1,2)
plot(f,unwrap(angle(T))*180/pi,'--')
grid on
hold on


end
```

# References

[1] Lin-Feng Chen, CK Ong, CP Neo, VV Varadan, and Vijay K Varadan. *Microwave electronics: measurement and materials characterization*. John Wiley & Sons, 2004.

[2] Agilent Technologies. Free space measurements seminar. Agilent Technologies, 2015.

[3] AG Gorriti and EC Slob. Synthesis of all known analytical permittivity reconstruction techniques of nonmagnetic materials from reflection and transmission measurements. *Ieee Geoscience and Remote Sensing Letters*, 2(4):433–436, 2005. doi:10.1109/LGRS.2005.853199.

[4] RA Fenner, EJ Rothwell, and LL Frasch. A comprehensive analysis of free-space and guided-wave techniques for extracting the permeability and permittivity of materials using reflection-only measurements. *Radio Science*, 47(1), 2012.

[5] Ugur Cem Hasar. A microwave method for noniterative constitutive parameters determination of thin low-loss or lossy materials. *IEEE Transactions on Microwave Theory and Techniques*, 57(6):1595–1601, 2009.

[6] J Van der Ziel. Effect of fabry-perot interference on second harmonic generation in a gaas plate. *IEEE Journal of Quantum Electronics*, 12(7):407–411, 1976.

[7] Florence Sagnard, Faroudja Bentabet, and Christophe Vignat. In situ measurements of the complex permittivity of materials using reflection ellipsometry in the microwave band: theory (part i). *IEEE transactions on instrumentation and measurement*, 54(3):1266–1273, 2005.

[8] Florence Sagnard, Faroudja Bentabet, and Christophe Vignat. In situ measurements of the complex permittivity of materials using reflection ellipsometry in the microwave band: Experiments (part ii). *IEEE transactions on instrumentation and measurement*, 54(3):1274–1282, 2005.

[9] MR Benson, AG Knisely, MA Marciniak, MD Seal, and AM Urbas. Permittivity and permeability tensor extraction technique for arbitrary anisotropic materials. *IEEE Photonics Journal*, 7(3):1–13, 2015.

[10] Lionel Duvillaret, Frederric Garet, and J-L Coutaz. A reliable method for extraction of material parameters in terahertz time-domain spectroscopy. *IEEE Journal of selected topics in quantum electronics*, 2(3):739–746, 1996.

[11] A Pashkin, M Kempa, H Nemec, F Kadlec, and P Kuzel. Phase-sensitive time-domain terahertz reflection spectroscopy. *Review of Scientific Instruments*, 74(11):4711–4717, 2003. doi:10.1063/1.1614878.

[12] WB WEIR. Automatic measurement of complex dielectric-constant and permeability at microwave-frequencies. *Proceedings of the Ieee*, 62(1):33–36, 1974. doi:10.1109/PROC.1974.9382.

[13] Ugur Cem Hasar. Permittivity measurement of thin dielectric materials from reflection-only measurements using one-port vector network analyzers. *Progress In Electromagnetics Research*, 95:365–380, 2009.

[14] S Arslanagić, Troels Vejle Hansen, N Asger Mortensen, Anders Heidemann Gregersen, Ole Sigmund, Richard W Ziolkowski, and Olav Breinbjerg. A review of the scattering-parameter extraction method with clarification of ambiguity issues in relation to metamaterial homogenization. *IEEE Antennas and Propagation Magazine*, 55(2):91–106, 2013.

[15] SS STUCHLY and M MATUSZEWSKI. Combined total reflection-transmission method in application to dielectric-spectroscopy. *Ieee Transactions on Instrumentation and Measurement*, 27(3):285–288, 1978. doi:10.1109/TIM.1978.4314682.

[16] AM NICOLSON and GF ROSS. Measurement of intrinsic properties of materials by time-domain techniques. *Ieee Transactions on Instrumentation and Measurement*, IM19(4):377–, 1970. doi:10.1109/TIM.1970.4313932.

[17] Osman S Ahmed, Mohamed A Swillam, Mohamed H Bakr, and Xun Li. Efficient optimization approach for accurate parameter extraction with terahertz time-domain spectroscopy. *Journal of Lightwave Technology*, 28(11):1685–1692, 2010.

[18] Shenhui Jing, Yao-Jiang Zhang, Jing Li, Dazhao Liu, Marina Y Koledintseva, David J Pommerenke, Jun Fan, and James L Drewniak. Extraction of permittivity and permeability for ferrites and flexible magnetodielectric materials using a genetic algorithm. *IEEE Transactions on Electromagnetic Compatibility*, 57(3):349–356, 2015.

[19] Ugur Cem Hasar, Joaquim José Barroso, Yunus Kaya, Mehmet Ertugrul, Musa Bute, and José M Catalá-Civera. Two-step numerical procedure for complex permittivity retrieval of dielectric materials from reflection measurements. *Applied Physics A*, 116(4):1701–1710, 2014.

[20] H. Nemec, F. Kadlec, P. Kuzel, L. Duvillaret, and J. L. Coutaz. Independent determination of the complex refractive index and wave impedance by time-domain terahertz spectroscopy. *Optics Communications*, 260(1):175–183, 2006. URL: <GotoISI>://WOS:000236500000030, doi:10.1016/j.optcom.2005.10.019.

[21] JM Catala-Civera, F Penaranda-Foix, D Sanchez-Hernandez, and E de los Reyes. A simple procedure to determine the complex permittivity of materials without ambiguity from reflection measurements. *Microwave and Optical Technology Letters*, 25(3):191–194, 2000. doi:10.1002/(SICI)1098-2760(20000505)25:3<191::AID-MOP10>3.0.CO;2-5.

[22] Ugur Cem Hasar, Joaquim Jose Barroso, Cumali Sabah, and Yunus Kaya. Resolving phase ambiguity in the inverse problem of reflection-only measurement methods. *Progress In Electromagnetics Research*, 129:405–420, 2012.

[23] Ugur Cem Hasar and Charles Roger Westgate. A broadband and stable method for unique complex permittivity determination of low-loss materials. *IEEE transactions on Microwave Theory and Techniques*, 57(2):471–477, 2009.

[24] Zsolt Szabo, Gi-Ho Park, Ravi Hedge, and Er-Ping Li. A unique extraction of metamaterial parameters based on kramers–kronig relationship. *IEEE Transactions on Microwave Theory and Techniques*, 58(10):2646–2653, 2010.

[25] Elena Saenz, Luis Rolo, Maurice Paquay, Giampiero Gerini, and Peter de Maagt. Sub-millimetre wave material characterization. In *Proceedings of the 5th European Conference on Antennas and Propagation (EUCAP)*, pages 3183–3187. IEEE, 2011.

[26] J Sanz-Fernandez, E Saenz, and L Rolo. Microwave material characterization free-space test facility. In *35th ESA Antenna Workshop on Antenna and Free Space RF Measurements*, 2013.

[27] Luis Rolo, Eric van der Houwen, and Elena Saenz. Characterization of reflectivity losses in space reflector antennas at temperatures above 350°c.

[28] E Saenz, L Rolo, K van't Klooster, M Paquay, and VV Parshin. Accuracy assesment of material measurements with a quasi-optical free-space test bench. In *2012 6th European Conference on Antennas and Propagation (EUCAP)*, pages 572–576. IEEE, 2012.

[29] Clean Room Classifications. http://www.cleanairtechnology.com/cleanroom-classifications-class.php. Accessed: 2010-09-30.

[30] Kenneth Levenberg. A method for the solution of certain non-linear problems in least squares. *Quarterly of applied mathematics*, 2(2):164–168, 1944.

[31] Donald W Marquardt. An algorithm for least-squares estimation of nonlinear parameters. *Journal of the society for Industrial and Applied Mathematics*, 11(2):431–441, 1963.

[32] Daniel Bourreau, Alain Péden, and Sandrick Le Maguer. A quasi-optical free-space measurement setup without time-domain gating for material characterization in the-band. *IEEE transactions on instrumentation and measurement*, 55(6):2022–2028, 2006.

[33] UKAS website. https://www.ukas.com/download/publications/publications-relating-to-laboratory-accreditation/M3003_Ed3_final.pdf. Accessed: 2010-09-30.

[34] James W Lamb. Miscellaneous data on materials for millimetre and submillimetre optics. *International Journal of Infrared and Millimeter Waves*, 17(12):1997–2034, 1996.

[35] PEEK dielectric properties of peek™ polymer. http://www.cgtec.eu/wp-content/uploads/dielectric-properties-450G-GL30-vs-T-and-f-e.pdf. Accessed: 2010-09-30.

[36] EVONIK rohacel datasheet. http://www.rohacell.com/sites/lists/RE/DocumentsHP/ROHACELL-Dielectric-Properties-EN.pdf. Accessed: 2010-09-30.